Maria Inês de Jesus Duarte Farrim

Licenciada em Biologia – Ramo de Biologia Molecular e Genética

Triggering of intracellular aggregation and cytotoxicity by immature forms of human Islet Amyloid Polypeptide

Dissertação para obtenção do Grau de Mestre em
Genética Molecular e Biomedicina

Orientador: Doutora Regina Menezes Echaniz, PhD, Chronic Diseases Research Center, Faculdade de Ciências Médicas, Universidade Nova de Lisboa

Co-Orientador: Doutora Margarida Castro-Caldas Braga, PhD, Faculdade de Ciências e Tecnologias, Universidade Nova de Lisboa

Júri:

Presidente: Prof. Doutora Alexandra Fernandes (FCT-NOVA)

Arguente: Doutora Catarina Pimentel (ITQB-NOVA)

Vogal: Doutora Regina Menezes (CEDOC-NOVA Medical School/Faculdade de Ciências Médicas)

FACULDADE DE CIÊNCIAS E TECNOLOGIA
UNIVERSIDADE NOVA DE LISBOA

Dezembro, 2020

Maria Inês de Jesus Duarte Farrim

Licenciada em Biologia – Ramo de Biologia Molecular e Genética

Triggering of intracellular aggregation and cytotoxicity by immature forms of human Islet Amyloid Polypeptide

Dissertação para obtenção do Grau de Mestre em
Genética Molecular e Biomedicina

Orientador: Doutora Regina Menezes Echaniz, PhD, Chronic Diseases Research Center, Faculdade de Ciências Médicas, Universidade Nova de Lisboa

Co-Orientador: Doutora Margarida Castro-Caldas Braga, PhD, Faculdade de Ciências e Tecnologias, Universidade Nova de Lisboa

Júri:

Presidente: Prof. Doutora Alexandra Fernandes (FCT-NOVA)

Arguente: Doutora Catarina Pimentel (ITQB-NOVA)

Vogal: Doutora Regina Menezes (CEDOC-NOVA Medical School/Faculdade de Ciências Médicas)

FACULDADE DE CIÊNCIAS E TECNOLOGIA
UNIVERSIDADE NOVA DE LISBOA

Dezembro, 2020

Triggering of intracellular aggregation and cytotoxicity by immature forms of human Islet Amyloid Polypeptide

Part of the results discussed in this thesis were presented in the following scientific journal and meeting:

Scientific journal:

Raimundo, A. F., Ferreira, S., Farrim, M. I., Santos, C. N., & Menezes, R. (2020). Heterologous Expression of Immature Forms of Human Islet Amyloid Polypeptide in Yeast Triggers Intracellular Aggregation and Cytotoxicity. Frontiers in Microbiology, 11, 2035.

Poster communications:

Ana Filipa Raimundo, Sofia Ferreira, Maria Inês Farrim, Cláudia Nunes dos Santos, Regina Menezes. 2020. "Effects of IAPP processing in aggregation and cell viability". Paper presented in 16º Congresso da Sociedade Portuguesa de Diabetologia (SPD) [selected by the scientific committee for oral discussion by Sofia Ferreira], Portugal.

This work was performed in Molecular Nutrition and Health Group, at CEDOC – Chronic Diseases Research Center, NOVA Medical School. It was supported by Nuno Castel-Branco award from the Portuguese Diabetes Society (SPD), UID/Multi/04462/2013-SubProj Inova4health 44 for the project "TherDIAPP_Islet Amyloid Polypeptide oligomers as critical entities in diabetes: early diagnosis and therapeutic", and PTDC/BIA-MOL31104/2017 for the project "Therapeutics@DIAPP_Perceiving Diabetes as an Islet Amyloid PoliPeptide oligomeropathy: disease progression and therapeutic focus".

ACKNOWLEDGEMENTS

First of all, I would like to thank the Scientific Committee of the MSc in Molecular Genetics and Biomedicine of Nova School of Science and Technology (FCT NOVA) for the planning and organization of this course and to Chronic Diseases Research Center (CEDOC) of Nova Medical School for receiving me as a master student and allowing me to work on this project. I would also like to thank Dr. Cláudia Nunes dos Santos for welcoming me into the group and for letting me develop this work in her lab. I am grateful for all the input with her scientific approach.

To my supervisor Dr. Regina Menezes I thank her for all the patience, guidance and support. I am grateful for the opportunity to join this project and for all the trust along this journey. For all the encouragement and enthusiasm, but also for being strict and demanding when needed. To my co-supervisor, Prof. Dr. Margarida Braga, I thank her for all the availability, dedication, and reassurance.

A huge thank you to all my lab colleagues, Andreia, Rita, Rafael, Diogo, Daniela, Zé Diogo and Catarina who made me feel so welcomed and included in the group. Thank you for creating a great work environment and for all the encouragement. It was my pleasure to work alongside you. A huge special thanks to Ana and Sofia, whom I cherish for being my tutors and guiding me through all this process. I cannot thank you enough for all that you have done and for all you taught me. Thank you for all the enthusiasm and support and for always being there for me. You all made this journey more pleasurable and memorable.

To my friends, I cannot thank you enough. To my “big sister” Mariana for all the patience in the world and for listening. I could not ask for a better friend. For all the stories, pieces of advice, words of encouragement and long hours side by side writing. And we did it! Thank you so much for always being there for me, every step of the way, never letting me fall or feel alone. To my “little sister” Carol, thank you for all the cheering and constant support. For all the good times we spent together and for always listening.

To Mónica and Carolina, with whom I shared the pains and joys of being a biology student, and with whom I can always count no matter what. Thank you for all that you have been teaching me and for always having my back. To Pedro and Dinis, for being my IT guys and an endless fountain of uplifting motivation and never ending belief in my abilities. To Rodrigo for still being here with me since the beginning of times and for being an inspiration all these years. To everyone in Fonte Santa who watched me grow and never failed to make me laugh, even in the darkest times. And to Gonçalo for all the unforgetful moments and belief.

I also want to thank everyone who, in one way or another, helped me on this journey and encouraged me to push forward and be the best I could be. Thank you for all the trust placed in me and in my abilities.

And of course, to my parents and my family for all their love and never ending support, giving me all the opportunities and encouraging me on. I would not be where I am without you. I hope I can make you proud.

ABSTRACT

Diabetes is a chronic metabolic disease with increasing numbers worldwide. Pancreatic deposits of human Islet Amyloid Polypeptide (hIAPP) represent the major histopathological hallmark of type 2 diabetes. IAPP is a hormone produced by β-cells, which is released upon glucose stimulation concomitantly with insulin, acting on gastric emptying and glycemic control. It is synthesized as preproIAPP (ppIAPP) hormone that is first processed to proIAPP (pIAPP) and finally to its mature form (matIAPP). Impairment in IAPP processing seems to be associated with the accumulation of immature IAPP forms, leading to the formation of toxic intracellular aggregates, which have been associated with β-cell dysfunction and loss. Currently, IAPP proteotoxicity is not fully understood. The main goals of this study were to investigate the pathological role of immature IAPP forms involved in intracellular aggregation and to test the potential protective activity of tauroursodeoxycholic acid (TUDCA) towards IAPP-induced cytotoxicity. To this end, *Saccharomyces cerevisiae* models recapitulating IAPP intracellular aggregation were characterized. Expression of human ppIAPP, pIAPP, and matIAPP fusions with green fluorescent protein (GFP) induced toxicity in yeast cells, with ppIAPP exerting the most deleterious effect on yeast growth and cell viability. Moreover, the expression of all IAPP constructs led to the formation of intracellular aggregates with different biochemical features. The first steps on generating a pancreatic β-cell line (INS-1) stably expressing hIAPP were also conducted. Overall, the data obtained suggest that the accumulation of immature hIAPP forms triggers the formation of highly cytotoxic intracellular aggregates. Although TUDCA has been shown to overcome proteotoxicity induced by amyloid proteins, neither TUDCA nor ursodeoxycholic acid (UDCA) were able to protect yeast cells against the toxic effects of hIAPP aggregates. These novel yeast models represent powerful tools for future research focused on IAPP-induced toxicity and to screen for compounds mitigating the deleterious effects caused by IAPP aggregation.

Keywords: Amylin, Diabetes, IAPP, Protein aggregation, *Saccharomyces cerevisiae*, TUDCA

RESUMO

A Diabetes é uma doença metabólica crónica, com números crescentes por todo o mundo. Os depósitos do polipeptídeo amiloide dos ilhéus pancreáticos humanos (hIAPP) representam a principal característica histopatológica da diabetes do tipo 2. IAPP é uma hormona pancreática produzida nas células β, que é secretada juntamente com a insulina em resposta à presença de glucose, atuando no controlo glicémico. É sintetizado na forma de preproIAPP (ppIAPP) que é primeiro processado em proIAPP (pIAPP) e finalmente na sua forma madura (matIAPP). Alterações no processamento do IAPP parecem estar associadas a uma acumulação de formas imaturas de IAPP, levando à formação de agregados intracelulares tóxicos, associados à perda das células β. Atualmente, a proteotoxicidade do IAPP não é totalmente compreendida. Os principais objetivos deste estudo foram desvendar o papel patológico das formas imaturas de IAPP envolvidas na agregação intracelular e testar a potencial atividade protetora do ácido tauroursodeoxicólico (TUDCA) na toxicidade induzida pelo IAPP. Assim, modelos de *Saccharomyces cerevisiae* que recapitulem a agregação intracelular de IAPP foram desenvolvidos e caracterizados. A expressão de fusões de ppIAPP, pIAPP e matIAPP humano com a proteína fluorescente verde (GFP) induziram toxicidade na levedura, com ppIAPP exercendo o efeito mais deletério no crescimento e viabilidade celular. A expressão de todas as construções de IAPP levaram à formação de agregados intracelulares com diferentes características bioquímicas. Os primeiros passos no desenvolvimento de uma linha de células β pancreáticas (INS-1) expressando hIAPP de forma estável também foram realizados. Assim, os dados sugerem que a acumulação de formas imaturas de hIAPP desencadeia a formação de agregados intracelulares citotóxicos. Embora o TUDCA tenha demonstrado melhorar a proteotoxicidade induzida por proteínas amilóides, nem ele nem o ácido ursodeoxicólico (UDCA) foram capazes de proteger as células de levedura contra os efeitos tóxicos dos agregados de hIAPP. Estes novos modelos representam ferramentas poderosas para investigações futuras com foco na toxicidade induzida por IAPP e no *screeening* de compostos que possam mitigar os efeitos deletérios causados pela agregação de IAPP.

Palavras-chave: Amilina, Diabetes, IAPP, Agregação de proteínas, *Saccharomyces cerevisiae*, TUDCA

TABLE OF CONTENTS

FIGURE INDEX

TABLE INDEX

ABBREVIATIONS

ATP	Adenosine Triphosphate
Blast	Blasticidin
cAMP	Cyclic Adenosine Monophosphate
cDNA	Complementary DNA
CMV	Human Cytomegalovirus
CPE	Carboxypeptidase E
CREB	cAMP Response Element-Binding Protein
DAG	Diacylglycerol
DM	Diabetes Mellitus
Dox	Doxycycline
ER	Endoplasmic Reticulum
GCK	Glucokinase
GFP	Green Fluorescent Protein
GLUT1	Glucose Transporter 1
GLUT2	Glucose Transporter 2
GLUT3	Glucose Transporter 3
GSIS	Glucose-stimulated Insulin Secretion
GWAS	Genome-Wide Association Studies
hIAPP	Human Islet Amyloid Polypeptide
IAPP	Islet Amyloid Polypeptide
IDE	Insulin-Degrading Enzyme
IDP	Intrinsically Disordered Protein
IP3	Inositol Triphosphate
matIAPP	Mature Islet Amyloid Polypeptide
mRNA	Messenger RNA
NASH	Non-alcoholic steatohepatitis
NEP	Neprilysin
PAM	Peptidylglycine Alpha-Amidating Monooxygenase
PC1/3	Prohormone Convertase 1/3
PC2	Prohormone Convertase 2
PCR	Polymerase chain reaction
PDX1	Pancreatic and duodenal homeobox 1
PKA/C	Protein Kinase A/C
PI	Propidium Iodide
pIAPP	Pro Islet Amyloid Polypeptide
ppIAPP	Prepro Islet Amyloid Polypeptide
PP	Pancreatic polypeptide
ROS	Reactive Oxygen Species

SLC2A1	Soluble Carrier Family 2 Member 1
SLC2A2	Soluble Carrier Family 2 Member 2
SLC2A3	Soluble Carrier Family 2 Member 3
SP	Signal Peptide
T1DM	Type 1 of Diabetes Mellitus
T2DM	Type 2 of Diabetes Mellitus
TCA	Tricarboxylic acid
TGN	Trans-Golgi Network
TUDCA	Tauroursodeoxycholic Acid
UDCA	Ursodeoxycholic Acid
UPR	Unfolded Protein Response
UTR	Untranslated Region

I. INTRODUCTION

I.1 Diabetes Mellitus – A Brief Overview

I.1.1 Epidemiology

Diabetes mellitus (DM), hereby referred to as diabetes, is a chronic metabolic disease that affects millions of people worldwide. In 2019, approximately 463 million adults (1 in 11 adults) between the ages of 20 to 79 were living with diabetes. It is estimated that this number will reach 700 million by 2045 (International Diabetes Federation, 2019). In Portugal, by 2015, 9,8% of the population between the ages of 25 and 74 had diabetes (Barreto et al., 2017). Furthermore, according to the National Diabetes Observatory's preliminary data, in 2018, this number already increased to 13,6% (National Diabetes Observatory, 2019).

In 2019, 4.2 million deaths all over the world were attributed to diabetes, and the number of people with the disease or at risk of developing this condition is rapidly increasing in most countries. Diabetes brings severe impacts on the world's economy and people's life-quality, becoming a growing public health problem (International Diabetes Federation, 2019). Of importance, diabetes often leads to other health complications such as vascular and neurological complications (Del Guerra et al., 2005; Kahn, 2003; Kahn et al., 2006). Therefore, there is an urgent necessity to uncover the early pathological causes of diabetes as to develop effective strategies allowing its control or prevention.

I.1.2 Classification

Diabetes is mainly characterized by elevated blood glucose levels (hyperglycaemia) and glucose intolerance due to insufficient insulin response (International Diabetes Federation, 2019; Kayatekin et al., 2018; Zou et al., 2019). However, this disease is also highly heterogeneous regarding its clinical presentation and progression (Ahlqvist et al., 2018).

Diabetes is generally classified into two most common types: type 1-diabetes mellitus (T1DM) and type 2-diabetes mellitus (T2DM). T1DM represents 5-10% of all diabetes cases and results in complete insulin insufficiency due to the destruction of insulin-producer β-cells by islet-cell antibodies (Rorsman & Braun, 2013; Del Guerra et al., 2005). On the other hand, T2DM counts for approximately 90% of the cases, mainly characterized by insufficient insulin secretion and insulin resistance (Zou et al., 2019). The underlying causes for the development of T2DM are still unknown and probably have multiple origins, both genetic and environmental, such as lifestyle factors (Haataja et al., 2008). (Ascroft & Rorsman, 2012). Genome-wide association studies (GWAS) show more than sixty common gene variants or loci, most of which play a role in β-cell function, that could increase the risk of developing T2DM (Rorsman & Braun, 2013). Additionally, a recent study showed that T2DM is remarkably highly heterogeneous, and there could be different subgroups with different characteristics and risks of diabetic complications (Ahlqvist et al., 2018). For example, it was identified a cluster of individuals with insulin-resistance with a high risk of diabetic kidney disease and a cluster of young insulin-deficient individuals with metabolic deficiencies demonstrating the high variability of this disease (Ahlqvist et al., 2018).

I.1.3 Glucose Homeostasis

Glucose homeostasis results from a tightly regulated system where the rise of blood glucose is compensated by insulin release by pancreatic β-cells (Raimundo et al., 2020). In healthy conditions, this feedback guarantees that the plasma glucose levels remain within the physiological range (between 3.5-5.5 mmol/L) (Guemes et al., 2016).

A human pancreas contains ~ 1 million pancreatic islets of Langerhans. These islets are quite heterogeneous in terms of composition, having different types of cells with different functions. Pancreatic β-cells are the most abundant endocrine cell type (~ 50%). These cells are responsible for the synthesis and secretion of insulin and IAPP, essential for maintaining glucose homeostasis. Besides β-cells, pancreatic islets are also composed of α-cells (35-40%), δ-cells (10-15%) responsible for glucagon and somatostatin release, respectively. Pancreatic polypeptide cells (F-cells) are also components of islets (< 5%) and are responsible for the secretion of pancreatic polypeptide (PP). ε-cells produce ghrelin and are less than 1% of islet secretory cells (Rorsman & Braun, 2013; Brereton et al., 2015; McGuckin et al., 2020) (**Figure I.1**).

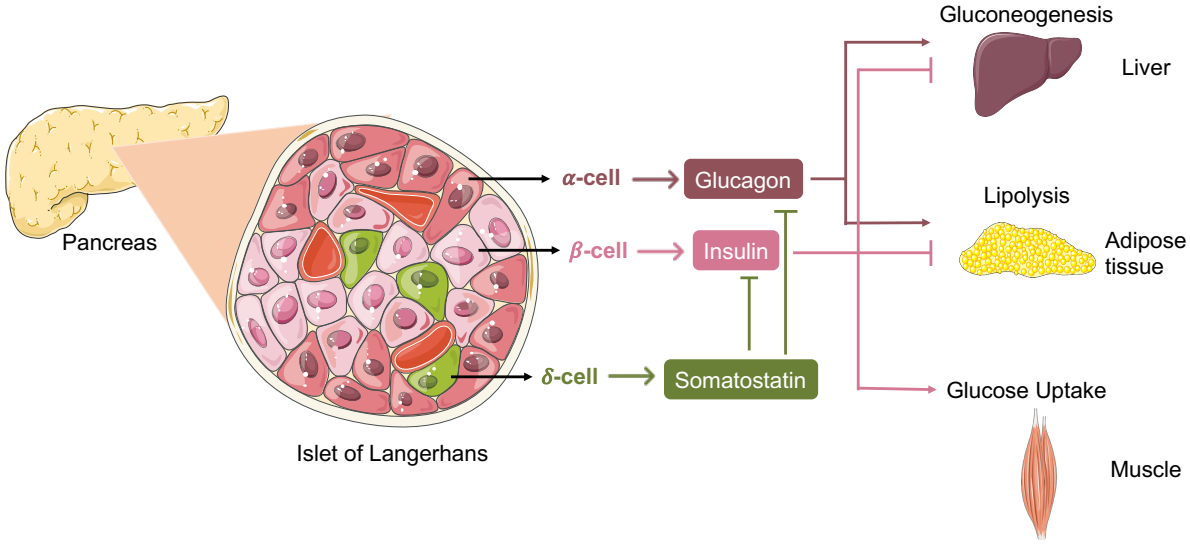

Figure I.1 – Schematic representation of the main secretory cells of pancreatic islets of Langerhans. Islets of Langerhans are mainly composed by β-cells (~ 50%), α-cells (35-40%) and δ-cells (10-15%). β-cells produce and secrete insulin, that promotes glucose uptake in muscle tissues, while inhibits liver gluconeogenesis and lipolysis in the adipose tissue. α-cells are responsible for the secretion of glucagon which has the opposite effect of insulin in liver and adipose tissue, promoting gluconeogenesis and lipolysis. δ-cells secrete somatostatin, which has an inhibitory effect on insulin and glucagon.

Insulin is an essential hormone in glucose regulation. It is mainly released in response to the intracellular uptake and glucose metabolism after food ingestion. The predominant glucose transporters in human β-cells are GLUT1 (encoded by *SLC2A1*), GLUT2 (encoded by *SLC2A2*) and GLUT3 (encoded by *SLC2A3*). Once in the cytosol, glucose metabolism begins with glucose phosphorylation, generating glucose 6-P, catalyzed by the rate-limiting enzyme glucokinase (GCK). This enzyme functions as a glucose sensor, having a relatively lower affinity for glucose than the other hexokinases (Fu et al., 2013) and is not inhibited by its own products. Additionally, loss-of-function mutations in this GCK gene result in this pathway's impairment (Rorsman & Braun, 2013). Glucose 6-P then enters the glycolysis pathway, whose end-products enter the oxidative phosphorylation pathway, that ends in ATP

production. Elevated levels of ATP inhibit the K^+ channels leading to depolarization of the cell membrane. The alteration of membrane potential activates the voltage-dependent calcium channels, causing a calcium influx, triggering insulin release via exocytosis. Although the increase in calcium influx triggers insulin exocytosis, other secondary signals like cAMP, IP3, DAG amplify this response (Ascroft & Rorsman, 2012; Fu et al., 2013; Xavier & Rutter, 2020) (**Figure I.2**).

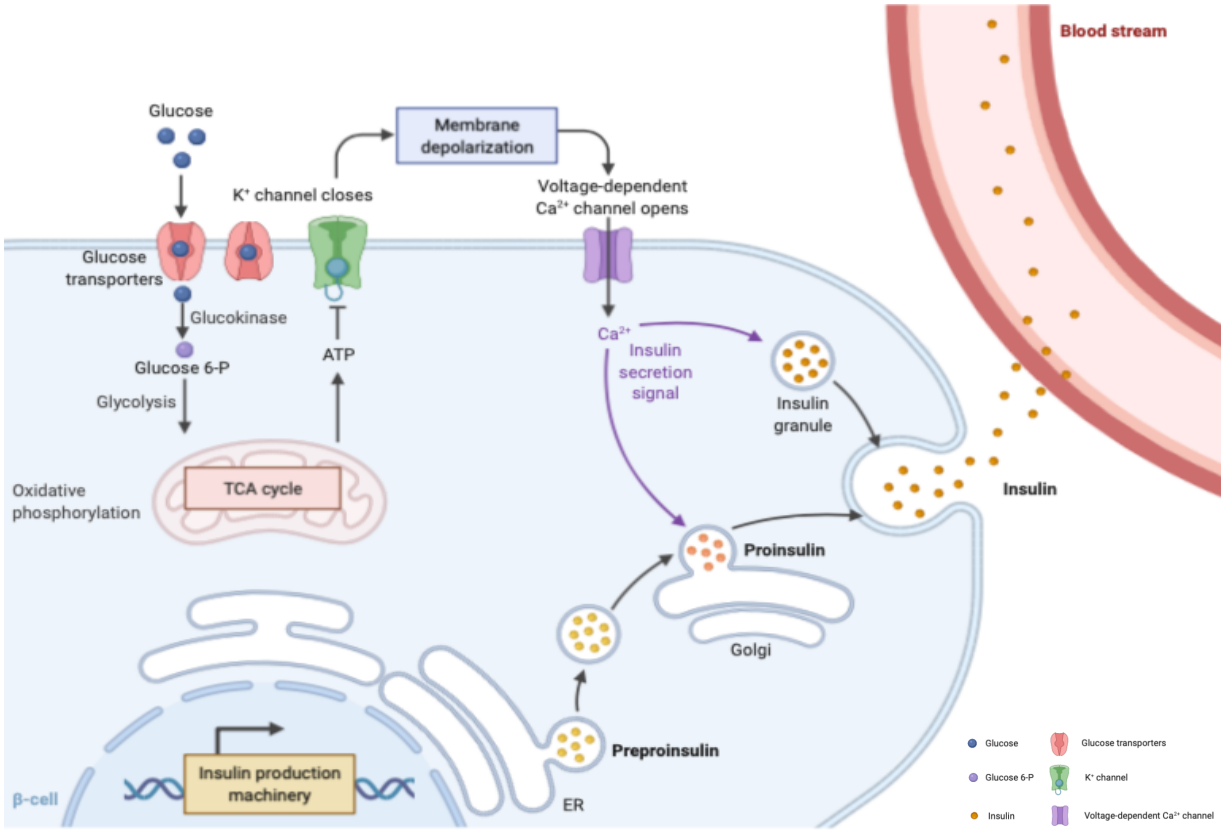

Figure I.2 – Schematic representation of glucose-induced insulin pathway in pancreatic β-cells. In β-cells, glucose is transported to the cytosol by specific transporters and phosphorylated by glucokinase to glucose 6-P. This compound enters the glycolysis pathway, whose end-products enter the oxidative phosphorylation pathway and ATP is produced. Rising levels of ATP inhibit K^+ channels leading to the depolarization of the cell membrane. The alteration of membrane potential activates the voltage-dependent calcium channels, causing a calcium influx, triggering the exocytosis of insulin into the blood stream. ATP = Adenosine triphosphate, ER = endoplasmic reticulum, TCA = Tricarboxylic acid. Image created with Biorender.com.

I.I.4 Pathogenesis

The pathogenesis of T2DM is highly complex and many aspects of its pathophysiology are still unknown. It is known that mutations in genes involved in β-cell physiology increase the risk of developing this disease (Rorsman & Braun, 2013). Moreover, lifestyle factors such as diet and obesity are known to influence β-cell function and peripheral insulin resistance. T2DM is thought to result of two major components: the development of insulin resistance and β-cell dysfunction/mass reduction (Rorsman & Braun, 2013).

Furthermore, in islets from patients with T2DM, glucose-induced insulin secretion is reduced by 60% when compared to healthy individuals due to an impairment in β-cell function. Besides, oxidative glucose metabolism is also compromised in these individuals, along with a reduction in GCK expression

(Rorsman & Braun, 2013). Furthermore, patients with T2DM often manifest β-cell mass reduction due to an increase in β-cell apoptosis (Fu et al., 2013).

Therefore, different causes for β-cell loss have been suggested, namely, glucolipotoxicity, endoplasmic reticulum (ER) stress, inflammation, and amyloid formation (Haataja *et al*., 2008). Glucolipotoxicity results of a chronic and extensive exposure of the pancreatic cells to high concentrations of glucose and fatty acids, with deleterious effects on β-cell function. Elevated concentrations of glucose overstimulate the insulin secretion pathway, disturbing the cells homeostasis and induces the production of reactive oxygen species (ROS) and inflammation. The β-cells are particularly vulnerable to oxidative stress, which can trigger signaling cascades resulting in cell death. So, when glucotoxicity happens, β-cell damage can lead to irreversible defects in insulin production and secretion (Fu et al., 2013). Furthermore, high glucose levels may interfere with fatty acid metabolism and promote the formation of toxic by-products. Besides, studies with fatty acids demonstrate that prolonged exposure to these molecules has impacts on insulin secretion. ER stress and the activation of the unfolded protein response (UPR) are also implicated in β-cell damage. Additionally, as the number of functional β-cells declines, islet amyloid deposits also seem to emerge, suggesting a relevant role of IAPP in β-cell dysfunction (Fu et al., 2013). All these toxic stimuli can create a huge metabolic burden in the ER and in the metabolic cellular pathways and create an unbalance that cannot be restored, resulting in cell death.

I.2 Diabetes as a Protein Misfolding Disorder

Changes in the correct folding of specific proteins can lead to the formation of aggregates and subsequent amyloid fibrils and plaques (**Figure I.3**). Protein misfolding is associated with several disorders, including T2DM. Amyloid formation was thought to be the leading cause of protein deposition-related diseases (Bucciantini et al., 2002; Knowles et al., 2014). Currently, oligomers are considered to be more toxic than the mature amyloid fibrils. They can interfere with essential cellular processes such as cell signaling, apoptosis, inflammation, and other cellular pathways culminating in cell death (Knowles et al., 2014).

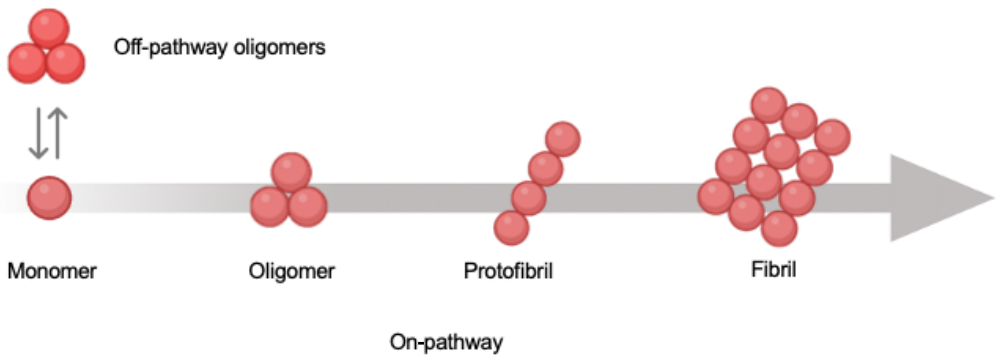

Figure I.3 – Schematic representation of amyloid fibril formation. Single monomers start aggregating leading to the formation of oligomers that turn into protofibrils, culminating in the formation of full mature fibrils. Monomers aggregation may follow alternative pathways giving rise to off-pathway oligomers that can interfere with crucial cell processes.

One important feature of diabetes is the aggregation of islet amyloid polypeptide (IAPP), which has been shown to have an essential role in the damage of pancreatic β-cells and disease progression. IAPP fibril deposits are histopathological hallmarks of T2DM, being present in the pancreas of 90% of patients (Mukherjee et al., 2017). IAPP aggregation is thought to be responsible for β-cell loss and for decline in β-cell function as demonstrated in post-mortem studies and islets transplants (Mukherjee et al., 2015). Studies in animal models (non-human primates and cats) that spontaneously develop T2DM demonstrated that the presence of IAPP aggregates precedes β-cell dysfunction and loss (Mukherjee et al., 2017). Furthermore, transgenic rodent models overexpressing human IAPP developed the pathological characteristics of T2DM, with formation of toxic intracellular oligomers of IAPP and deposition of IAPP (Mukherjee et al., 2015; Westermark et al., 2011; Lin et al., 2007). However, the link between IAPP pathogenicity and β-cell dysfunction is not completely understood (Kahn, 2003; Westermark et al., 2011).

I.2.1 Islet Amyloid Polypeptide

IAPP, also known as amylin, was discovered and isolated from islet tumor cells of patients. It consists of a polypeptide hormone co-expressed and co-secreted with insulin by pancreatic islet β-cells. Therefore, the release of IAPP closely mirrors that of insulin. The storage and secretion ratio IAPP:insulin is approximately 1:100 in healthy individuals (Hull et al., 2004; Denroche et al., 2018). Importantly, this ratio can increase to 1:20 in T2DM individuals due to alterations in insulin sensitivity and insulin resistance since both are subjected to the same regulatory mechanisms (Hull et al., 2004; Fernández, 2014; Knight et al., 2008). Indeed, since IAPP and insulin are co-secreted, it is thought that insulin resistance may be closely associated with IAPP aggregation since it leads to an increase in IAPP production (Mukherjee et al., 2017).

IAPP is a soluble protein and its single subunit/monomeric form state is unfolded. After its production, IAPP is mainly stored in the halo of the secretory granules and posteriorly secreted upon the stimulation with glucose and other secretagogues, like sulfonylureas. (Fernández, 2014; Cobb & Dukes, 1998). Under normal conditions, IAPP plays a role in glycemic regulation. It inhibits insulin secretion, increasing the blood glucose uptake and reducing the glucose output from the liver. IAPP also increases renin-activity and vasodilation, and slows gastric emptying, suppressing appetite (**Figure I.4**).

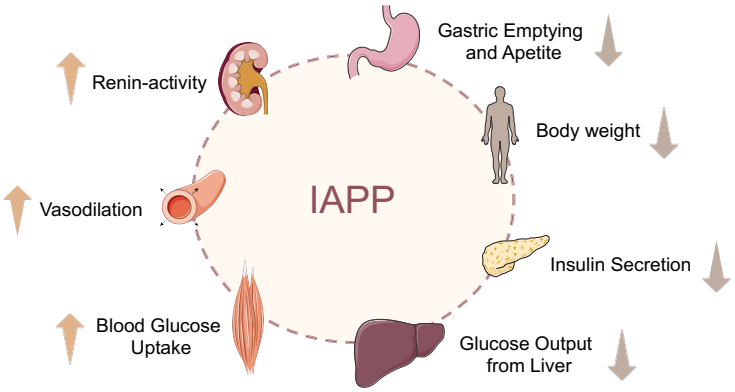

Figure I.4 – Physiological functions of human IAPP. IAPP plays a role in glycemic regulation. It inhibits insulin secretion, glucose output from liver, slows gastric emptying and suppresses appetite, decreasing body weight. It also promotes renin-activity, vasodilation and blood glucose uptake. IAPP = islet amyloid polypeptide (Adapted from Press et al., 2019).

I.2.2 Regulation of IAPP Expression

The human IAPP gene, located on the short arm of chromosome 12, belongs to the calcitonin family. It is present in all mammals, and there is a high homology of the mature IAPP sequence among the different species (Asthana et al., 2018).

The human IAPP gene contains three exons. The first exon is presumably a regulatory mRNA sequence encoding most of the 5'-untranslated region (UTR), while the second one includes the sequences for the initiation of translation, the signal peptide (SP), and a few amino acids that compose the N-terminus of preproIAPP (ppIAPP). The third exon contains the amino acids of the mature IAPP (matIAPP), an 3'-untranslated region, and the C-terminus of proIAPP (pIAPP). An Alu sequence of repetitive DNA is also present in exon 3 (Christmanson et al., 1990; Asthana et al., 2018; Nishi et al., 1989). Mutations in IAPP gene have been associated with increased T2DM susceptibility (Gasa et al., 2001).

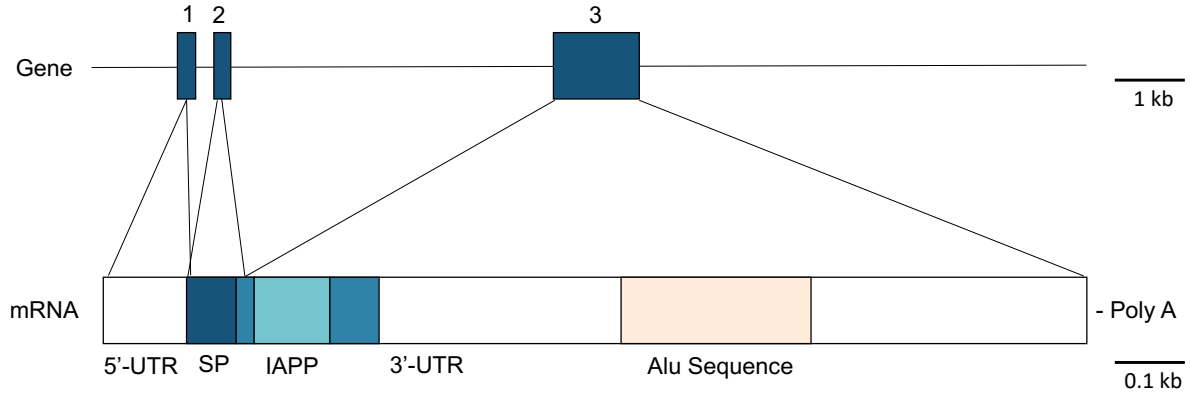

Figure I.5 – Schematic representation of the relationship between hIAPP gene and mRNA. The hIAPP gene is composed by the three exons represented by the respective number. The region of the mRNA encoded by each exon is indicated: 5'-UTR and 3'-UTR represent 5'- and 3'- untranslated regions of mRNA. IAPP represents the mature IAPP sequence and SP represents the signal peptide. mRNA of hIAPP also has an Alu sequence of repetitive DNA and the polyadenylation is represented by the tale of poly(A). IAPP = islet amyloid polypeptide, SP = signal peptide, UTR = untranslated region (Adapted from Nishi et al., 1989).

Several factors affect IAPP gene regulation. Peptide expression is regulated through the IAPP gene promoter, responsive to glucose but less sensitive than the insulin promoter (Fernández, 2014). The pancreatic and duodenal homeobox 1 (PDX1) transcription factor activates both insulin and IAPP promoters. The insulin gene is mainly activated following PDX1 modulation by glucose. However, the IAPP gene is not activated by PDX1 unless in the absence of calcium (Ca^{2+}) signaling. When Ca^{2+} signaling is restored, the IAPP gene becomes activated with the help of PDX1, indicating that glucose has a direct impact on the transcription of insulin and an indirect impact on IAPP transcription. Studies suggest an essential role of calcium and PKA/C signaling pathways in IAPP gene transcription (Macfarlane et al., 2000; Asthana et al., 2018).

I.2.3 IAPP and Insulin Processing

IAPP and insulin processing in β-cells are very similar since both hormones are processed by the same enzymes at the same location (Marzban et al., 2005). Generation of mature IAPP starts with the synthesis of the 89-residue IAPP precursor – ppIAPP – in β-cells. The ppIAPP hormone is

hydrolyzed by a signal peptidase in the ER to form a 67-residue pIAPP, which is cleaved at the two pairs of basic residues (Lys-Arg) located in the NH2 and COOH termini, by prohormone convertase 2 (PC2) and prohormone convertase 1/3 (PC1/3), respectively (Marzban et al., 2005). pIAPP dibasic residues are removed by the action of carboxypeptidase E (CPE) to form the mature IAPP consisting of 37 amino acids, which is stored in secretory granules. Other post-translational modifications include the formation of an intramolecular disulfide bridge between residues 2 and 7, and amidation of the C-terminus by peptidylglicine α-amidating monoxygenase (PAM) (**Figure I.6A**) (Westermark et al., 2011; Marzban et al., 2005; Marzban et al., 2006; Zou et al., 2019).

Similarly, insulin is first synthesized as the precursor – preproinsulin. This preprohormone' signal peptide is cleaved in the ER to yield proinsulin. Still within the ER, intramolecular disulfide bonds are formed between the peptide cysteine residues. Proinsulin is then cleaved by endoproteases PC1/3 and PC2 and CPE removes four amino acid residues to yield mature insulin, which is stored in the secretory granules (**Figure I.6.B**) (Bratanova-Tochkova et al., 2002).

PC1/3, PC2, PAM, CPE are all highly enriched in mature secretory granules, emphasizing their crucial role in prohormone processing. Expression of these enzymes is dynamically and tightly regulated at the transcriptional, translational, and posttranslational levels, and diabetogenic stressors have been shown to affect their regulation (Marzban et al., 2005; Paulsson et al., 2006; Chen et al., 2018).

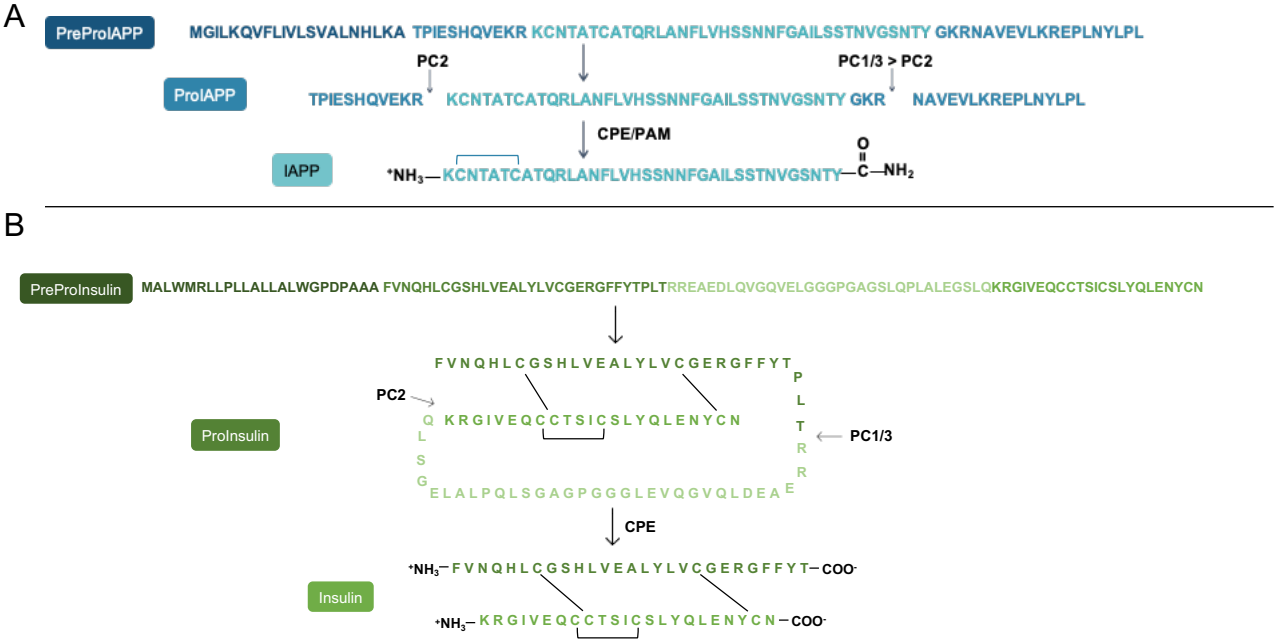

Figure I.6 – Processing pathway of human IAPP and insulin. (**A**) IAPP is synthesized as an 89-residue designated preproIAPP. The 22-residue signal sequence (dark blue) is cleaved to give rise to the 67-residue proIAPP. The N- and C-terminal proIAPP flanking regions are shown (blue). ProIAPP is then cleaved by the prohormone convertases PC1/3 and PC2 at two conserved dibasic sites. The C-terminus is amidated by PAM after processing by CPE resulting in the mature 37-residue IAPP. The biologically active peptide has a disulfide bridge between Cys-2 and Cys-7. (**B**) Insulin is first synthesized as preproinsulin. The signal peptide (dark green) is cleaved in the ER to yield proinsulin. There occurs the formation of disulfide bonds between the cysteine residues. Proinsulin is then processed by PC1/3 and PC2 at two conserved sites. Additionally, CPE removes four amino acid residues to yield mature insulin. IAPP = islet amyloid polypeptide, ER = endoplasmic reticulum, PC1/3 = prohormone convertase 1/3, PC2 = prohormone convertase 2, CPE = carboxypeptidase E, PAM = peptidylglicine α-amidating monoxygenase.

I.2.4 IAPP Secretion Pathways

Endocrine cells, such as pancreatic β-cells, possess two secretory pathways involved in the release of hormones: the regulated and the constitutive pathways. Prohormones are synthesized in the ER and are then transported to the trans-Golgi network (TGN) (Marzban et al., 2005). In the regulated secretory pathway, pro-proteins are sorted into secretory granules for processing and storage before their release by exocytosis. This process occurs in response to secretagogues. The constitutive secretory pathway is thought to be the default pathway by which newly synthesized pro-proteins exit the TGN in small vesicles to be rapidly released without storage. It is only regulated at the level of biosynthesis and is not subject to regulation by secretagogue (Marzban et al., 2005) (**Figure I.7**). Co-localization of IAPP and insulin in secretory granules suggested that they are both released via the regulated secretory pathway in normal conditions (Gasa et al., 2001). However, 90% of proinsulin is directed at the regulated pathway, while only 66% of pIAPP appeared to follow the same pathway. Indeed, studies suggest that the increase in IAPP production might overwhelm the regulated pathway and promote IAPP secretion via the constitutive pathway (Gasa et al., 2001). Under certain conditions, unprocessed forms of IAPP might also be secreted by both pathways, which could promote amyloid formation and deposition (Marzban et al., 2005; Marzban et al., 2006).

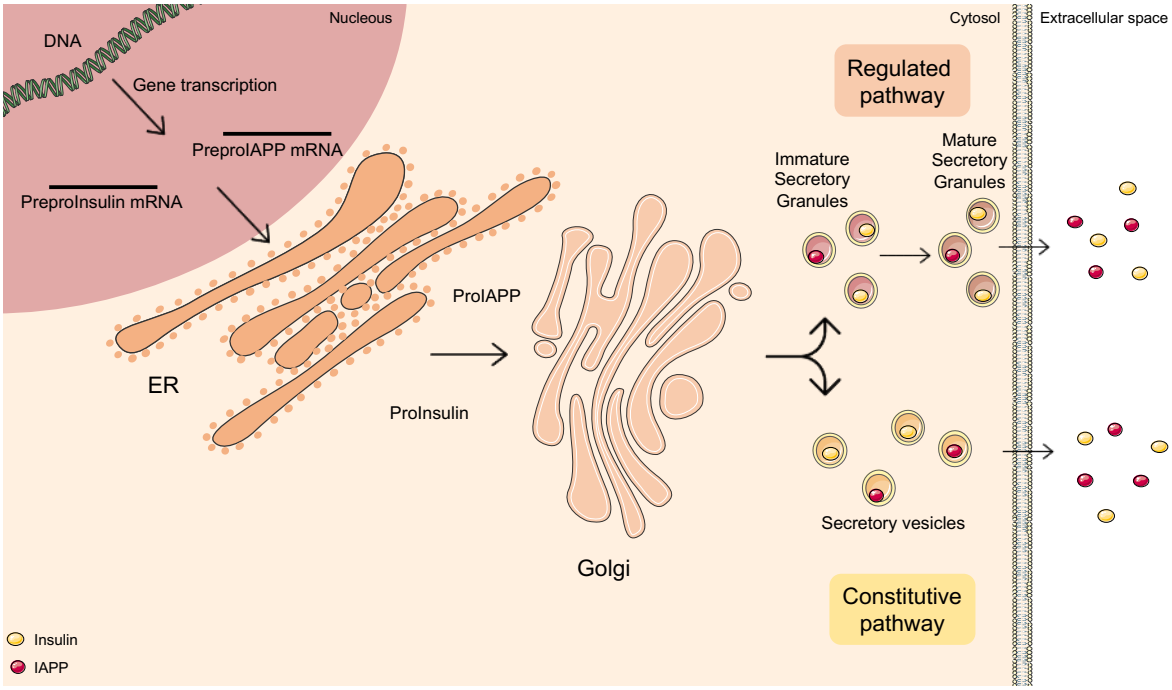

Figure I.7 – Schematic representation of IAPP and insulin secretion by the regulated and constitutive pathways. IAPP and insulin are synthesized in the ER and transported to the Golgi. Then they can follow two different secretion pathways. In the regulated secretory pathway, the hormones are sorted into secretory granules to finish processing and stored before their release by exocytosis. In the constitutive secretory pathway, the newly synthesized hormones exit the trans-Golgi network (TGN) in small vesicles that can be rapidly released without storage. IAPP = islet amyloid polypeptide, ER = endoplasmic reticulum (Adapted from Marzban et al., 2005).

I.2.5 IAPP Clearance

IAPP is removed from cells in different ways. The plasma clearance rates of IAPP and insulin differ as circulating IAPP is removed from plasma by renal excretion, by glomerular filtration and tubular secretion, being more slowly cleared than insulin (Hull et al., 2004; Leckström et al., 1997). Furthermore, β-cells have enzymes that can clear IAPP. However, little is known about the enzymes involved in this turnover. The insulin-degrading enzyme (IDE) is a protease with high-affinity for insulin that can also degrade IAPP, playing an important role in IAPP clearance (Bennett et al., 2000). Interestingly, mutations in IDE gene have been associated with T2DM susceptibility. Inhibition of IDE function enhanced IAPP aggregation in rat pancreatic β-cells (Mukherjee et al., 2015). Additionally, peptidase neprilysin (NEP) can also cleave and degrade IAPP, inhibiting oligomers, and fibrils formation by a non-catalytic interaction between the two proteins (Guan et al., 2012). Studies in mice overexpressing hIAPP showed elevated NEP levels, which can be a compensatory mechanism for the increase in IAPP production (Mukherjee et al., 2015, Zraika et al., 2007).

I.2.6 IAPP Amyloidogenic Properties

Amyloidogenesis is a process characterized by the spontaneous self-assembly of peptides into higher-order structures such as oligomers, protofibrils and mature fibrils (Raimundo et al., 2020). The monomeric form of IAPP is a natively or intrinsically disordered protein (IDP), meaning that, under physiological conditions, it lacks a stable or fixed tertiary structure. Instead, it can assume numerous configurations and can interact with different structures. Importantly, IDPs are usually aggregation-prone. Human IAPP, as well as IAPP from primates and cats, forms amyloid structures. The aggregation properties of IAPP are thought to be linked to the presence of proline residues. The most variable region is between residues S20 to S29, thought to be an important section in amyloidogenic propensity However, studies show that other sequence regions also interfere with IAPP aggregation (**Figure I.8**) (Fernández, 2014; Akter et al., 2015, Asthana et al., 2018).

Figure I.8 – **Alignment of preproIAPP sequences from human, rat, mouse, cat and primate**. The signal peptide is represented (dark blue), followed by proIAPP sequence (blue). The mature IAPP sequence (light blue) is shown with a square marking the most variable region, between residues S20 and S29 (Adapted from Asthana et al., 2018).

The kinetics of IAPP aggregation *in vitro* have been investigated in several studies. It starts with a slow nucleation phase, which is followed by a rapid increase in the aggregation rate and culminating in a fibrillogenic plateau. IAPP dimerization starts by the formation of α-helical structures that lead to the formation of β-hairpins and β-sheets that mainly compose the mature fibrils. Current hypothesis highlights the importance of oligomers and intermediate species as the main drivers of IAPP toxicity (Fernández, 2014; Westermark et al., 2011).

I.2.7 Molecular Mechanisms Underlying IAPP Cytotoxicity

IAPP cytotoxicity has been demonstrated *in vitro* and in animal models. Similar to findings of protein aggregates in neurodegenerative diseases, the consensus on the real toxic forms of IAPP has shifted from the amyloid deposits and large plaques to smaller and diffusible oligomers, which can infiltrate cellular membranes and alter essential cell functions. Recent findings show that these aggregates can be found intra- and extracellularly (Kayatekin et al., 2018; Asthana et al., 2018).

Intracellular IAPP oligomers disrupt multiple aspects of β-cell function. They can lead to ER stress, defects in the UPR, proteasome deficiency, autophagy impairment, inflammation, mitochondrial dysfunction, receptor-mediated mechanisms linked to oxidative stress, and activation of signaling cascades and cell membrane permeabilization resulting in β-cell apoptosis. All these processes promote islet amyloidosis and disease progression. Besides, receptor-mediated mechanisms of IAPP toxicity support the pathological role of extracellular oligomers, suggesting that they can bind to receptors and activate the inflammasome. Thus, IAPP-mediated cytotoxicity can be activated by extra- and intracellular oligomers (Abedini & Schmidt, 2013; Raleigh et al., 2017) (**Figure I.9**).

Remarkably, the ER has a vital role in protein synthesis and post-translational modifications, including their correct folding and assembly (Cao et al., 2016; Chung et al., 2017). It is also the intracellular organelle that senses environmental changes and cellular stress, being very susceptible to factors that alter its homeostasis, leading to ER stress (Chung et al., 2017). Several factors such as accumulation of unfolded or misfolded proteins, ROS, free fatty acids, and hyperglycaemia lead to ER stress (Cao et al., 2016; Chung et al., 2017). It has been shown that pancreatic β-cells are particularly susceptible to ER stress, mainly because they have an extremely developed ER due to their high protein synthesis and secretion rate. Moreover, several studies point to ER stress as a critical mechanism involved in β-cell dysfunction and T2DM progression associated with extra- and intracellular IAPP aggregation (Huang et al., 2019). Additionally, oxidative stress has been linked to diabetes pathophysiology in animal models and humans (Baynes & Thorpe, 1999; Kucharska et al., 2000). Several authors believe that liver damage (steatohepatitis) described in T1DM and T2DM and non-alcoholic steatohepatitis (NASH) is due to mitochondrial dysfunction closely dependent on oxidative stress, which is enhanced in diabetic animals and patients (Lukivskaya et al., 2007).

One of the most widely accepted hypothesis indicate that IAPP-induced cytotoxicity occurs via a membrane disruption mechanism. IAPP oligomers are mainly composed of α-helical structures and can penetrate and anchor the membrane to form a hollow tubular structure leading to pores' formation, disrupting plasma and organelle membranes, ultimately leading to apoptosis (Abedini & Schmidt, 2013; Zou et al., 2017). These findings are compatible with the hypothesis that cell death occurs when the expression of unprocessed IAPP exceeds β-cells capacity to process it, resulting in an accumulation of toxic, partially processed forms that aggregate and interfere with essential cellular pathways.

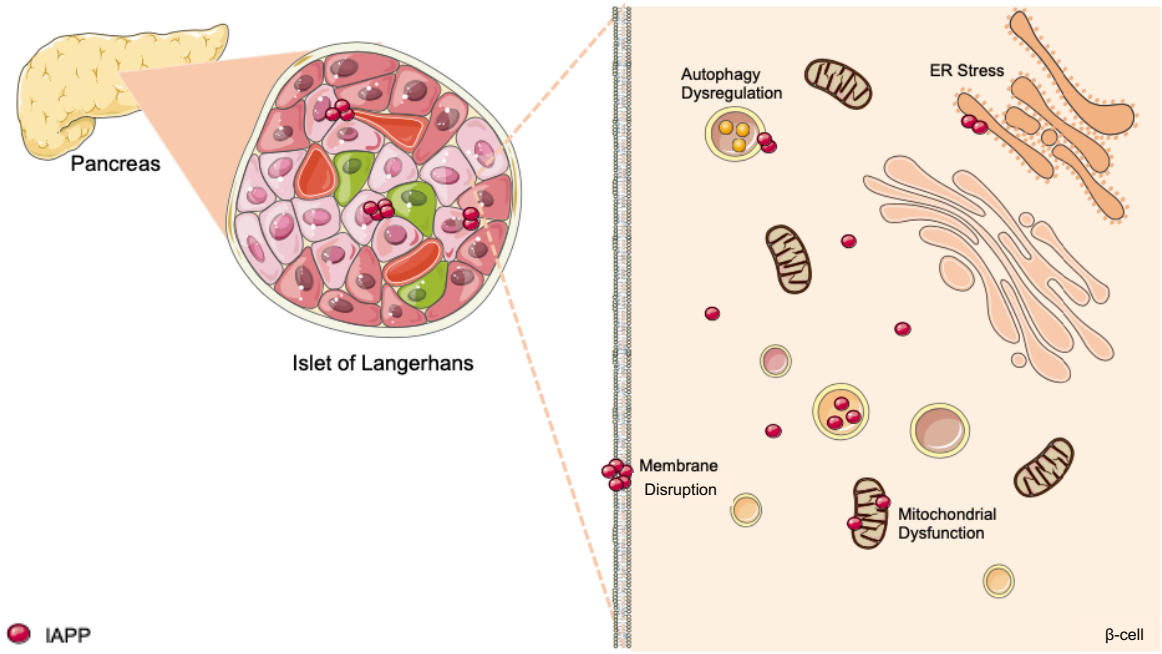

Figure I.9 – Possible molecular mechanisms underlying IAPP-induced toxicity. Intracellular IAPP aggregates may disrupt multiple aspects of β-cell function, leading to ER stress, defects in the UPR, proteasome deficiency, autophagy impairment, inflammation, mitochondrial dysfunction, oxidative stress, activation of signaling cascades and cell membrane permeabilization resulting in β-cell apoptosis. Extracellular aggregates can form amyloid deposits damaging pancreatic tissue. ER = endoplasmic reticulum, UPR = unfolded protein response, IAPP = islet amyloid polypeptide.

I.3 Experimental Models of IAPP Proteotoxicity

Over the years, several experimental models have been used in diabetes research (Rees & Alcolado, 2005). Non-mammalian animal models, like *Caenorhabditis elegans*, *Drosophila melanogaster* and zebrafish, have the advantage of having a low maintenance cost, a short life cycle, and various gene-editing tools available. However, their translational value to the human is limited, considering the differences in physiology. On the other side, larger animal models such as dog, pig, and non-human primates, are closer to human physiology but are a lot harder to maintain and have long life cycles with a few offspring. Rodents emerged as a compromise between throughput and translational value since their physiology is relatively similar to humans and are easier to maintain and study (Kleinert et al., 2018).

On the other side, the contribution of *in vitro* models have been very relevant in the diabetes field. As human islets are laborious to maintain, human β-cell lines have been an important tool for understanding β-cells physiology. However, these lines are still unstable, less physiologic and sensible, becoming difficult to manipulate under laboratory conditions (Andersson et al., 2015; Green et al., 2018). As a consequence of these limitations, and despite the physiological differences between rodent and human β-cell lines (Green et al., 2018), recombinant rodent β-cell lines have been widely used to better understand β-cell physiology. Thus, there is currently no ideal β-cell model to address the intricacies of pancreatic β-cell dysfunction observed in T2DM (Zou et al., 2019; Hohmeier et al., 2000).

I.3.1 INS-1 Pancreatic β-cell Line

Several attempts have been made to design stable insulin-secreting cell lines. The most widely used cells lines are from radiation- or virus-induced insulinomas such as β-hyperplastic islet-derived cells derived from preneoplastic islet cells or rat insulinoma cell line (RIN) and insulinoma cell line (INS-1) generated from irradiated cells (Skelin et al., 2010).

The INS-1 rat cell line has been used as a model for metabolic signaling mechanisms in the β-cell, having a higher response to glucose over the physiological range than the other cell models (Hohmeier et al., 2000).

Asfari et al. (1995) isolated the cell line INS-1 832/13 from a heterogeneous population of parental INS-1 cells with different glucose-sensing capacities and stably transfected them with a plasmid containing the human insulin gene under the control of the cytomegalovirus promoter and a neomycin resistance gene. Remarkably, the clone 832/13 had a stable and robust response to glucose-stimulated insulin secretion (GSIS) similar to the physiological response. This enhanced secretory responsiveness to glucose can be maintained for a few months in culture, suggesting its potential for studying the mechanisms of insulin secretion and drug screening of therapeutic compounds diabetes (Hohmeier et al., 2000). Therefore, this INS-1 832/13 cell line arises as an optimized model to study the processes inherent to β-cells that are altered in diabetes. However, cell lines are complex and challenging to manipulate and it has not been developed a cell line model optimized to study all the aspects of IAPP cytotoxicity.

I.3.2 Yeast Model of Protein Aggregation

Saccharomyces cerevisiae is a simple eukaryotic organism that has been widely used as a model for the study of human diseases. It presents several advantages over the other experimental models. Being very versatile with a short generation time, it is easily manipulated and maintained under laboratorial conditions (Smith & Snyder, 2006).

S. cerevisiae was the first eukaryotic organism to have its genome fully sequenced. This achievement allowed the development of a myriad of genetic and biochemical tools and resources, such as, yeast gene deletion strains, inducible and repressible systems to generate conditional mutants, two-hybrid system, strains engineered to overexpress heterologous recombinant proteins, among others (Menezes et al., 2015; Smith & Snyder, 2006).

Remarkably, this yeast's genome has approximately 1000 genes orthologous to mammalians and associated with human diseases, enabling the study of specific aspects of several human diseases (Menezes et al., 2015). The high evolutionary conservation of fundamental biological processes among eukaryotes make yeast a powerful model for the study of human diseases. Cell cycle, transcription and translation, protein processing, clearance and proteostasis mechanisms, vesicular trafficking, autophagy, cytoskeleton dynamics, organelle biogenesis and metabolism are some of the molecular processes that are shared between yeast and higher eukaryotes (Menezes et al., 2015; Smith & Snyder, 2006). Particularly, protein folding is a critical process for cell survival, consequently, cellular mechanisms conserved from yeast to humans have evolved to ensure that proteins are correctly folded. Thus, yeast can provide a valuable tool to explore the mechanisms behind aberrant protein misfolding

and aggregation (Menezes et al., 2015; Tenreiro & Outeiro, 2010). This makes yeast an ideal model in interrogating the intricacies of human protein misfolding diseases. For instance, heterologous expression of disease-associated proteins has been used to investigate cellular responses and disease pathological mechanisms (Outeiro & Muchowski, 2004; Smith & Snyder, 2006).

Yeast models expressing human proteins associated with several disorders capture key aspects of cellular pathology and have allowed major advances in understanding the fundamental pathological processes of human diseases (Khurana & Lindquist, 2010; Menezes et al., 2015). In the particular regard of IAPP, a recent study disclosed the first model of IAPP toxicity in yeast strains expressing IAPP oligomers triggering toxicity, ER stress and impairing ER transport. These models advanced the state of the art in the diabetes field, however, many aspects of IAPP proteotoxicity remain to be investigated and yeast models emerge as unprecedented tools to investigate several molecular aspects underlying IAPP aggregation and cytotoxicity (Kayatekin et al., 2018).

I.4 Bile Acid Effects in Diabetes

Bile acids are molecules derived from cholesterol and originated in hepatic cells (Vettorazzi et al., 2016). They play a role in the digestion and absorption of dietary lipids and fat-soluble vitamins, regulate cholesterol excretion and sterol homeostasis. They can also have a role as extracellular messengers in many tissues, including the pancreas (Vettorazzi et al., 2016). Previous studies suggest that their chemical structure may influence their bioactivity (Martinez et al., 1998; Hofmann & Roda, 1984), and they recently emerged as important regulators of glucose and lipid metabolism (Cao et al., 2016).

I.4.1 Ursodeoxycholic acid (UDCA) and the Taurine-conjugate (TUDCA) Protective Functions

Ursodeoxycholic acid (UDCA), a bile acid, and the taurine-conjugate (TUDCA) act as chemical chaperones that ameliorate ER stress (Chung et al., 2017) (**Figure I.10**). They have been extensively used in the treatment of different liver diseases, and have therapeutic potential in non-liver diseases, such as neurological, retinal, metabolic, and myocardial disorders (Chung et al., 2017; Lukivskaya et al., 2007; Vettorazzi et al., 2016). Moreover, increasing evidence in neurodegenerative disorders points to a role of these chaperones in preventing the protein aggregation to attenuate ER stress (Cadavez et al., 2014; Vettorazzi et al., 2016).

UDCA is a primary component of black bear bile and has been used in clinic for the treatment of liver diseases over the years. It has a wide range of cellular actions, including anti-apoptotic and anti-inflammatory effects in hepatocytes (Chung et al., 2016). It has beneficial effects on hepatic steatosis, insulin resistance, and enhancement of ER adaptive capacity (Cao et al., 2016). Previous studies demonstrated that UDCA could modulate the apoptotic pathway by preventing membrane perturbations/regulating mitochondrial functions with ROS reduction in hepatic and non-hepatic cells from various non-bile acid agents. The *in vivo* studies suggest that bile acids directly or indirectly modulate apoptosis-related protein abundance at the mitochondrial membrane (Rodrigues et al., 1998). UDCA alleviated ER stress, which resulted in the normalization of hyperglycaemia and restoration of

systemic insulin sensitivity, thereby revealing their potential benefits in treating type 2 diabetes (Özcan et al., 2006). UDCA improved the morphology of pancreatic β-cells and restored the amount of cytoplasmic secretory granules of insulin-producing β-cells, which resulted in increased insulin production and prevented hyperglycemia in a rat model of alloxan-induced diabetes (Lukivskaya et al., 2004).

TUDCA is a chemical chaperone resulting from the natural conjugation of UDCA with taurine and it is produced in very small amounts. The taurine groups are known to enhance bioavailability of the compound (Invernizzi et al., 1999), so it is expected that TUDCA has a greater protective effect. It is a well-known inhibitor of ER stress, thereby improving protein folding. Studies in experimental models of obesity have reported that TUDCA can act as a chemical chaperone that ameliorates insulin resistance by reducing ER stress, stabilizing protein conformation, improving the ER folding capacity and the UPR. Additionally, studies in mouse pancreatic islets show that TUDCA can stimulate insulin secretion in a glucose-dependent manner by a mechanism mediated by the cAMP/PKA/CREB pathway (Cadavez et al., 2014; Vettorazzi et al., 2016). Furthermore, TUDCA treatment was shown to prevent β-cell dysfunction and maintain insulin secretory response in a similar way to untreated cells. Other evidences indicate that the activation of ER stress markers was reversed after treatment with this chaperone, and in thapsigargin or high glucose/palmitic acid treatment, the addition of TUDCA prevents activation of ER-stress protein markers. Importantly, results obtained using the hIAPP-INS1E cell line demonstrate that TUDCA treatment ameliorates insulin secretory response (Cadavez et al., 2014).

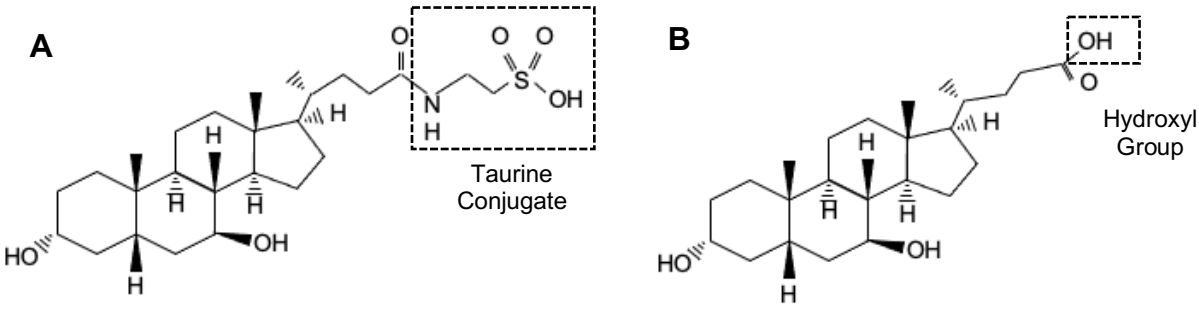

Figure I.10 – **Chemical structure of TUDCA and UDCA**. (**A**) TUDCA and (**B**) UDCA. The frames represent the differences between the two compounds. UDCA = ursodeoxycholic acid, TUDCA = tauroursodeoxycholic acid.

I.5 Aims

Given the importance of IAPP proteotoxicity in T2DM, understanding the mechanisms controlling IAPP processing and secretion from β-cells is critical. There is still a lot to unveil regarding the molecular mechanisms behind IAPP-induced toxicity. This may help identify new possible therapeutic targets to inhibit islet amyloid formation and lead to a better understanding of the disease.

The main objective of this study was to understand the role of immature IAPP species in formation of intracellular aggregates by developing eukaryotic models facilitating the investigation of the mechanisms associated with IAPP processing and aggregation. The final goal was to investigate

the potential protective activity of the chaperone UDCA and its taurine derivative TUDCA towards IAPP-mediated proteotoxicity.

To achieve these aims, the following intermediate goals were proposed:

- To ascertain the pathological role of immature forms of human IAPP in yeast models (Task 1);
- To develop an INS-1 832/13 rodent β-cell line stably expressing immature hIAPP for the validation of yeast results (Task 2);
- To evaluate the potential protective effect of the chaperones UDCA and TUDCA (Task 3).

II. MATERIALS AND METHODS

II.1 Materials

II.1.1 Chemicals

Several kits were used in this study, namely, In-Fusion® HD Cloning System (Takara Clontech, Japan), ZR Plasmid Miniprep-Classic and Zymoclean Gel DNA Recovery Kit (Zymo Research, USA), MicroBCA kit (Thermo Fisher Scientific, USA), Cell Titer-Blue® Cell viability assay (Promega, USA).

Yeast extract, tryptone and peptone were obtained from BD Biosciences, USA. Linear Hygromycin Marker 2 µg and Doxycycline were purchased from Takara Bio, Japan. Ethylenediaminetetraacetic acid (EDTA), 1,4-Dithiothreitol >99% (DTT), glycerol, ampicillin and galactose were obtained from Sigma®, Germany. GeneRuler 1 kb DNA Ladder, GeneRuler 100 bp DNA Ladder, Dimethylsulfoxide (DMSO), agarose, methanol and sodium-pyruvate were acquired from ThermoFischer Scientific, USA. Bovine Serum Albumin (BSA), Tween 20, denatured DNA from salmon sperm, Trichloroacetic acid (TCA), Hydrochloric Acid (HCl), lithium acetate (LiAc), raffinose, glucose and 2-mercaptoethanol from Sigma-Aldrich, USA. Phosphatase Inhibitor Cocktail Tablets and Protease Inhibitor Cocktail Tablets from Roche, Switzerland. Trypsin, phosphate buffer saline (PBS), Opti-MEM, RPMI-1640, HEPES, L-glutamine, DMEM and penicillin-streptomycin were obtained from GibcoTM, USA. Sodium dodecyl sulfate (SDS), Urea and N, N, N, N'-Tetramethyl ethylenediamine (TEMED) were purchased from Merck, Germany. Acrylamide, glycine and Tris were purchased from Carl Roth, Germany. For mammalian cell transfection, FuGene® HD Transfection Reagent was obtained from Promega, USA and Lipofectamine 2000 Reagent (1 mg/mL) from Invitrogen, USA. GreenSafe Premium was purchased from NZYTech, Portugal and ECL™ Prime Western Blotting System from GE Healthcare, USA. Acetone and isopropanol were acquired from Acros Organics, USA. Acetic acid, NaCl and protein marker VI (10-245) prestained from PanReac Applichem, Germany and agar from Prolab Scientific, Canada. Yeast nitrogen base (YNB) without amino acids from Difco, USA and single amino acid dropout CSM-URA from MP Biomedicals, USA. Fetal bovine serum (FBS) was obtained from Biowest, France. Tauroursodeoxycholic acid (TUDCA) and Ursodeoxycholic acid (UDCA) were kindly provided by Dr. Margarida Braga.

II.1.2 Equipment

All the experimental procedures involving bacteria and yeast cell handling were performed in sterile conditions using a Labgard Class II biological Safety Cabinet. The experimental procedures with mammalian cells were performed in a Biological safety cabinet class 2 – Mars, Labo-Gene™. Bacteria and yeast cells were incubated in Excella E24 Incubator Shaker from New Brunswick Scientific and in a 200 IC incubator from Agitorb. DNA was quantified in Nanodrop (Thermo Fisher Scientific, USA). Readings of the OD600 were performed in 96-well plates (Thermo Fisher Scientific, USA) using a Biotek Power Wave XS Microplate Spectrophotometer (Biotek®, Winooski, USA) and absorbance and fluorescence readings were carried out using a Synergy™ HTX Multi-Mode Microplate Reader. Images

from western blot, filter trap and phenotypic assays were acquired using ChemidocTM XRS and ImageLab® software. GFP fluorescence was visualized using a Carl Zeiss LSM 710 (for confocal fluorescence microscopy) and a Leica Z2 fluorescence microscope and images were analyzed using Fiji-ImageJ1.51j8, USA. Flow cytometry was performed using a CyFlow Cube 6 (Sysmex Partec GmbH, Goerlitz, Germany), equipped with a blue solid-state laser (488 nm), green fluorescence channel (530/30 nm) and orange-red fluorescence channel (610/20 nm). Data analysis was performed using FlowJo software. Mini-PROTEAN Tetra cell system, Trans-Blot® SD semi-dry transfer system and Mini Trans-Blot® Electrophoretic Transfer Cell from Bio-Rad, USA were used in immunoblotting procedures. Thermocycler T3000 (Biometra, Germany) was used for the synthesis of cDNA. Centrifuges (Eppendorf, Germany) and thermomixer (VWR) were used when necessary.

II.1.3 Culture Media

Bacteria were cultured in liquid [5 g/L yeast extract, 10 g/L tryptone, 10 g/L NaCl] or solid [5 g/L yeast extract, 10 g/L tryptone, 10 g/L NaCl, 20 g/L agar] Luria-Broth (LB) media supplemented or not with the appropriated antibodies.

For yeast cell assays, the following media were used: YPD [20 g/L peptone, 20 g/L glucose, 10 g/L yeast extract], Synthetic dropout (SD)-glucose medium [0.67% (w/v) YNB, 0.77 g/L CSM-URA, 2% (w/v) glucose], SD-raffinose medium [0.67% (w/v) YNB, 0.77 g/L CSM-URA, 1% (w/v) raffinose], SD-galactose [0.67% (w/v) YNB, 0.77 g/L CSM-URA, 2% (w/v) galactose]. To prepare solid media, 2% of agar was used.

For INS-1 832/13 cells the medium used was RPMI-1640 media supplemented with 10% FBS, 10 mM HEPES, 2 mM L-glutamine, 1 mM sodium-pyruvate, 0.05 mM 2-mercaptoethanol. As for HeLa cells, DMEM High Glucose media supplemented with 10% FBS and 10% Penicillin-Streptomycin was used.

II.1.4 Strains and Plasmids

The bacteria strain used in this study was Escherichia coli (E. coli) XL1-Blue *recA1 endA1 gyrA96 thi-1 hsdR17 supE44 relA1 lac [F´ proAB lacIqZ∆M15 Tn10 (Tetr)]*. The yeast strain used in this study was BY 4741 *MATa his3Δ1 leu2Δ0 met15Δ0 ura3Δ0* (obtained from EUROSCARF). The mammalian cell lines used in this study were INS-1 832/1 stably expressing pCMV-Tet3G marker (INS-1 832/13 Tet3G), previously constructed in the lab and HeLa Tet-On® 3G (Takara Bio, Japan).

The plasmids used are listed in **Table II.1**.

Table II.1 – List of plasmids used in this study.

Plasmid	*Description*	*Source or reference*
*p426-Gal1**	*$GAL1_{promoter}$, 2µ, URA*	ATCC® 87341™
p426-SP	*$GAL1_{promoter}$-SP, 2µ, URA*	Raimundo et al. (2020)
p426-GFP	*$GAL1_{promoter}$-GFP, 2µ, URA*	Raimundo et al. (2020)
p426-SP-GFP	*$GAL1_{promoter}$-SP-GFP, 2µ, URA*	Raimundo et al. (2020)
p426-ppIAPP-GFP	*$GAL1_{promoter}$-ppIAPP-GFP, 2µ, URA*	Raimundo et al. (2020)
p426-pIAPP-GFP	*$GAL1_{promoter}$-pIAPP-GFP, 2µ, URA*	Raimundo et al. (2020)
p426-matIAPP-GFP	*$GAL1_{promoter}$-matIAPP-GFP, 2µ, URA*	Raimundo et al. (2020)
p426-ppIAPP	*$GAL1_{promoter}$-ppIAPP, 2µ, URA*	Raimundo et al. (2020)
p426-pIAPP	*$GAL1_{promoter}$-pIAPP, 2µ, URA*	Raimundo et al. (2020)
p426-matIAPP	*$GAL1_{promoter}$-matIAPP, 2µ, URA*	Raimundo et al. (2020)
pTRE3G-IRES	*$TRE3G_{promoter}$-IRES2, pUC, amp^R*	Clontech®
pTRE3G-ppIAPP-GFP	*$TRE3G_{promoter}$-ppIAPP-GFP, pUC, amp^R*	Raimundo et al. (manuscript under preparation)
pTRE3G-GFP	*$TRE3G_{promoter}$-GFP, pUC, amp^R*	Raimundo et al. (manuscript under preparation)

Note: * Empty plasmid used as control, ATCC = American Type Culture Collection, IAPP = islet amyloid polypeptide, SP = signal peptide, GFP = green fluorescent protein, ppIAPP = preproIAPP, pIAPP = pIAPP, matIAPP = mature IAPP, ampR = ampicillin resistant.

The yeast vectors expressing matIAPP, pIAPP and ppIAPP fused or not to GFP were previously constructed by digestion of p426-Gal-aSyn-GFP (Outeiro & Lindquist, 2003) with *Spe*I/*Hin*dIII to remove aSyn. The cDNA sequence of each form of IAPP was amplified by PCR and cloned into this vector using the In-Fusion Cloning kit. The same strategy was used to construct the vectors p426-SP-GFP and p426-SP. Briefly, the annealing of the respective primers was made for 5 min at 55 ºC and it was confirmed by agarose digestion. The vectors p426-Gal1 and p426-Gal1-hIAPP-GFP were also digested with *Spe*I/*Hin*dIII for 1 h at 37 ºC and purified with the kit Zymoclean™ Gel DNA Recovery Kit from the agarose gel.

For the plasmids used in mammalian cells, they were previously constructed by cloning the cDNA of ppIAPP-GFP into the pTREG vector using the kit mentioned above. The same strategy was used for GFP alone by replacing the ppIAPP sequence with the sequence corresponding to GFP.

Analytical 2% agarose gels were used to monitor the restriction patterns of DNA. The GeneRuler 1 kb DNA Ladder and GeneRuler 100 bp DNA Ladder were used as molecular weight markers.

II.1.5 Antibodies

The set of antibodies used in this study is shown in the table below (**Table II.2**). All antibodies were diluted in PBS-T with 5% BSA.

Table II.2 – List of antibodies used in this study.

Antibody	*Source*	*Identifier*	*Concentration*
Rabbit anti-IAPP polyclonal	Sigma-Aldrich	Cat# HPA053194	1:2500
Mouse anti-GFP	NeuroMabs	Cat# 75-131	1:5000
Mouse anti-Pgk1 monoclonal	Invitrogen	Cat# 459250	1:1000
Goat anti-mouse polyclonal peroxidase-conjugated	Sigma-Aldrich	Cat# A5278	1:10000
Stabilized goat anti-rabbit HRP-conjugated	Pierce	Cat# 1858415	1:5000

II.2 Methods

II.2.1 Bacteria Transformation and Plasmid DNA Purification

E. coli was used for cloning and plasmid propagation. Cells were grown in LB supplemented with 0.1 mg/mL of ampicillin for selection, under orbital agitation at 200 rpm. For the transformation, 10-100 ng of DNA were added to 40 µL of competent *E. coli* suspension and incubated on ice for 30 min, followed by incubation at 42 ºC for 1 min and 2 min incubation on ice, for thermal shock. Cells were then resuspended in 1 mL of LB and incubated for 1 h at 37 ºC, with orbital agitation at 200 rpm. Cells were plated onto LB agar media supplemented with selective antibiotic marker. After incubation overnight at 37 ºC, single colonies were inoculated in 2 mL of liquid LB media supplemented with antibiotic for plasmid DNA extraction and incubated overnight at 37 ºC at 200 rpm (Froger et al., 2007).

The kit ZR Plasmid Miniprep-Classic was used for plasmid DNA isolation according to manufacturer's instructions. Briefly, the bacterial culture was centrifuged and the indicated buffers were used for cell lysis and neutralization. The resulting solution was centrifuged and the supernatant was transferred to a Zymo-SpinTM IIN column and washed. The plasmid DNA was then eluted and quantified in Nanodrop.

Analytical 2% agarose gels were used to monitor plasmid DNA restriction patterns. The GeneRuler 1 kb DNA Ladder and GeneRuler 100 bp DNA Ladder were used as molecular weight markers. Plasmid DNA was stored at -20 ºC.

II.2.2 Yeast Competent Cells and Transformation

Yeast transformation procedures were carried out as indicated using the LiAc standard method (Gietz & Schiestl, 1991). Cell cultures were incubated in YPD overnight at 30 ºC under orbital agitation at 200 rpm diluted until a final optical density at 600 nm (OD_{600}) of 0.1 ± 0.01 (logarithmic growth phase) was obtained.

The following equation was used to synchronize the cultures:

$$OD_i \, x \, V_i = \frac{OD_f}{2(^t/_{gt})} \, x \, V_f \qquad \textbf{Equation II.1}$$

where OD_i is the initial optical density of the culture, V_i is the initial volume of culture, OD_f is the final optical density of the culture, t is the time (usually 16 h), gt is the generation time of the strain and V_f is the final volume of culture (Raimundo et al., 2020).

Cell cultures were incubated for approximately 4 h, centrifuged (4000 rpm, 5 min) and cells were resuspended in 1 mL of sterile H_2O and transferred to microtubes. Cells were centrifuged at 8000 rpm for 1 min and the supernatant was discarded. The pellet was resuspended in 1 mL of a solution of Tris-EDTA (TE)/LiAc [Tris 0.1 M; EDTA 10 mM; 100 mM LiAc]. Cells were centrifuged again and resuspended in TE/LiAc. The transformation mixture was prepared as follows: 5 µL of denatured DNA from salmon sperm; 0.5-1 ng of DNA; 50 µL of competent cells, 300 µL of PEG solution [40% PEG3350; 1x TE; 100 mM LiAc].

Cell suspensions were first incubated for 30 min at 30 ºC and then for 20 min at 42 ºC. Cells were washed with 1 mL of sterile H_2O, centrifuged at 4000 rpm 2 min and plated into (SD)-glucose medium. Plates were incubated for 48 h at 30 ºC.

II.2.3 Mammalian cells transfection

INS-1 832/13 Tet3G and HeLa Tet-On® 3G were maintained in T-75 flasks in RPMI media with supplements and in DMEM media with supplements, respectively. Cells were kept in a 37 °C humidified incubator with 5% CO_2 and were split every 3-4 days, when they obtained a confluence of 80-90%.

INS-1 832/13 Tet3G cells were transfected with the pTREG vectors as indicated in **Table II.1**. For that, cells were seeded in 6-well plates (1 x 10^6 cells/well) and kept at 37 °C with 5% CO_2. FuGene was the transfection agent used and manufacture's protocol was followed. Briefly, 2 µg of plasmid DNA and 4 µg of hygromycin linear marker and 6 µL of FuGene were added to Opti-MEM. The mixture was incubated for 30 min at room temperature and 200 µL of the reaction was added to each well. After 4 h, the media was changed, 1 µg/µL Doxycycline was added, and 24 h after the cells were observed for GFP fluorescence.

For HeLa Tet-On® 3G transfections, the same plasmid DNA was used. Cells were seeded in 24-well plates (0.1 x 10^6 cells/well) or 96-well plates (1,68 x 10^4 cells/well) and kept at 37 °C with 5% CO_2. Lipofectamine was the transfection agent used and manufacture's protocol was followed. Shortly, 1 µg of plasmid DNA and 4 µL of Lipofectamine were each added to 100 µL of Opti-MEM. The mixture was incubated for 10 min at room temperature and 36 µL or 6 µL of the reaction were added to each well on a 24-well plate or 96-well plate, respectively. After 4 h, the media was changed, 1 µg/µL Doxycycline was added, and 24 h after the cells were observed for GFP fluorescence.

II.2.4 Yeast Growth Conditions

Synthetic dropout (SD)-glucose medium was used to grow the cells transformed with p426-derived plasmids previously mentioned. For all experiments, an isolated colony was inoculated in SD-raffinose medium and cultures were incubated overnight at 30 ºC under orbital shaking at 200 rpm. Cultures were diluted in fresh medium and, unless indicated otherwise, they were incubated under the

same conditions until an OD_{600} of 0.5 ± 0.05 (logarithmic growth phase) was obtained. Then, cell cultures were diluted as indicated for each assay. In all experiments, repression or induction of constructs was carried out in SD-glucose or SD-galactose media, respectively.

II.2.5 Growth Curve Analysis

For the growth curves, yeast cultures were diluted to OD_{600} 0.05 ± 0.005 in SD-glucose and SD-galactose and incubated at 30 ºC with shaking for 24 h. Growth was monitored hourly by measuring OD_{600}.

The data was analyzed using a model-free spline (nonparametric) and a model fitting (parametric) approach was used to calculate the growth parameters in the R software. The package grofit (Kahm et al., 2010) was used to adjust a model-free spline and the parameters maximum cell growth (µm), length of the lag phase (lag time) were estimated from the spline fit. Grofit was also used to adjust a model-based and the parameters were estimated from the best model fit. The 95% confidence intervals (95CI) were calculated via bootstrapping for both model-free spline and model-based fits.

II.2.6 Phenotypic Growth Assays

For the phenotypic growth assays, yeast cells were grown in SD-raffinose medium to OD_{600} 0.4 ± 0.04 and then OD_{600} was adjusted to 0.1 ± 0.01. Serial dilutions were performed with a ratio of 1:3, and 5 µL of each dilution was spotted onto solid SD-medium containing glucose or galactose as the sole carbon sources. Growth was recorded after 48 h and 72 h incubation at 30 ºC (Lee et al., 2007).

II.2.7 Fluorescence Microscopy

Cell cultures were diluted to OD_{600} 0.1 ± 0.01 in SD-galactose, incubated at 30 ºC for 12 h under orbital agitation, and centrifuged at 3000 g for 3 min. Slides were prepared using 4 µL of cell suspensions.

II.2.8 Flow Cytometry

Cell cultures were diluted to OD_{600} 0.1 ± 0.01 in SD-galactose and incubated at 30 ºC for 3 h, 6 h, 9 h, 12 h and 24 h under orbital agitation. Cells were incubated in a 96-well plate with Propidium Iodide (PI) at a final concentration of 5 µg/mL for the last 30 min of the time point at 30 ºC under orbital agitation and protected from light. A minimum of 100 000 events were collected for each experiment. Cell doublets exclusion was performed based on Forward-A and -W scatter parameters. Results were expressed as the percentage of PI and GFP positive cells as compared to the control (Deere et al., 1998; Haase & Reed, 2002).

Additionally, assays with the compounds UDCA and TUDCA were performed. Cell cultures were diluted to OD_{600} 0.1 ± 0.01 in SD-galactose and incubated for 12 h with UDCA (10 µM, 30 µM, 50 µM, 70 µM) or TUDCA (100 µM, 250 µM or 500 µM). The consecutive steps were followed as described above.

II.2.9 Protein Extraction and Quantification

Yeast cell cultures were diluted to OD_{600} 0.1 ± 0.01 in SD-galactose and incubated at 30 ºC under orbital agitation. Two different cell protein extraction protocols were used.

For the Tris-based (TBS) [Tris 2.4 g/L, 8 g/L NaCl, pH 7.6] protein extraction, cells were collected by centrifugation for 4 min at 2500 g, the pellets were resuspended in TBS buffer supplemented with protease and phosphatase inhibitors, cells were disrupted with glass beads (Sigma, Germany) (3 cycles of 30 sec in the vortex and 2 min on ice) and cell debris were removed by centrifugation at 700 g for 3 min. Total protein was quantified using the MicroBCA kit according to the manufactures' instructions. Briefly, the MicroBCA working reagent and sequential standards of diluted BSA were prepared. In a 96-well plate, 150 µL of each standard or diluted sample were pipetted in duplicates and 150 µL of working reagent was added to each well. The plate was incubated for 2 h at 37 ºC and OD_{562} was monitored on Biotek Power Wave XS Microplate Spectrophotometer. The standard curve was obtained by plotting the average blank-corrected OD values for each BSA standard versus its concentration, allowing the determination of protein concentration.

For TCA protein extraction, the same cell culture volume was centrifuged at 10000 g for 5 min. The pellets were resuspended in 1 mL of 10% TCA and kept at -20 ºC overnight. Cells were centrifuged at 15000 g for 3 min and washed twice with 1 mL of acetone. The pellets were air-dried and resuspended in 200 µL of MURB [0.5% β-mercaptoethanol, 0.129 mM sodium azide, protease and phosphatase inhibitors] buffer. Cells were disrupted with glass beads (3 cycles of 30 sec in the vortex and 5 min on ice) and incubated at 70 ºC for 10 min. Cell debris were removed by centrifugation at 10000 g for 1 min and the supernatant was collected to a new tube (Wright et al., 1989).

To monitor secreted IAPP, cell media was collected by centrifugation and protein was extracted using TCA (Brissette et al., 2012). TCA in 10% (v/v) acetone 9:1 was added to each sample and incubated overnight at -20 ºC. Samples were centrifuged at 15000 g 10 min at 4 ºC and washed with cold acetone containing 20 mM DTT until the pellet became white. The pellets were air-dried and resuspended in sample buffer [8 M urea in Tris-HCl 1 M pH = 8 (+ SDS 1% | 1:1 and 1x inhibitor of proteases)].

For protein extraction from mammalian cells, cells were trypsinized, collected and samples were centrifuged at 200 g for 5 min. Cells were washed with PBS and diluted in RIPA buffer [150 mM NaCl, 0.5% Sodium Deoxycholate, 0.1% SDS, 50 mM Tris HCl pH 8] with protease and phosphatase inhibitors. Samples were incubated at 4 ºC for 45 min (vortex every 15 min), centrifuged at 4 ºC for 15 min at 15000 g and the supernatant was retrieved (Ngoka, 2008; Sekhon et al., 2015).

II.2.10 SDS-PAGE and Immunoblotting

Protein extracts from yeast cells were incubated at 95 ºC for 10 min before SDS-PAGE. Equal concentrations of total protein were loaded and resolved in Mini-Protean TGX Gels (Bio-Rad, USA) for 90 min at 90 V. Gels were transferred to PVDF membranes using the semi-dry transfer method. Membranes were activated with methanol and blocked with 5% (w/v) BSA dissolved in PBS-T [Tris 2.4 g/L, 8 g/L NaCl, 0.1% (v/v) Tween 20] for 1 h at room temperature with shaking. The primary antibodies against GFP, IAPP and Pgk1, were probed overnight at 4 ºC, according to **Table II.2**. The membranes

incubated with anti-IAPP were boiled in PBS for 3 min before blocking. All membranes were then washed 6 x 5 min in PBS-T and incubated with the appropriate secondary antibody (**Table II.2**) for 1 h at room temperature. The membranes were washed 6 x 5 min in PBS-T and incubated with ECL™ Prime Western Blotting System. Specific protein signals were normalized against the Pgk1 signal.

For protein extracts from yeast cell media or mammalian cells, equal amounts of protein were separated on a Tris-Tricine gel electrophoresis, during approximately 90 min, at 100 V. Gels were transferred to PVDF membrane activated with methanol, during 90 min, at 60 V and the same procedure was performed as described above. Results from lysates from extracellular media were normalized to Amido black protein stain.

II.2.11 Filter-trap Assays

Protein lysates were prepared and quantified as previously indicated. Increasing concentrations (5, 10 and 50 ug) of total protein were diluted in 1% (v/v) SDS in PBS and loaded onto a 0.22 µm pore nitrocellulose membrane (GE Healthcare, USA), pre-equilibrated with PBS in slot-blot apparatus. The samples were applied to the slot-blot apparatus and filtered by vacuum and the slots were washed twice with 1% (v/v) SDS in PBS. The membranes were blocked 1 h at room temperature with 8% BSA dissolved in PBS-T and incubated overnight with anti-IAPP primary antibody at 4 ^{o}C, according to **Table II.2**. The membranes were washed 6 x 5 min in PBS-T and incubated with ECL (Cox & Ecroyd, 2017; Juenemann et al., 2015).

II.2.12 Metabolic Capacity

The Cell Titer-Blue® Cell viability assay was used to monitor mammalian cell viability, according to manufactures' instructions. Cells were transfected in a 96-well plate, medium was removed, and cells were washed with PBS. Fresh medium with Cell Titer-Blue® reagent (20 µL in 100 µL of medium) was added to the cells followed by incubation at 37 ^{o}C with 5% CO_2 for 1 h. Fluorescence (560/590 nm) was monitored in Synergy™ HTX Multi-Mode Microplate Reader.

II.3 Statistical analysis

The results reported in this study are the average of at least three independent biological replicates and are represented as the mean ± SD. Differences among treatments were assessed by a 2-way ANOVA test using GraphPad Prism 7. R software was used to analyze data from growth curves.

III. RESULTS

III.1 Effects of Immature Forms of IAPP in Yeast Cellular Homeostasis

III.1.1 Engineering Yeast Models to Study the Role of Immature IAPP Forms on Aggregation and Proteotoxicity

To study the impact of immature IAPP forms on cell homeostasis, it was developed a set of yeast models expressing different IAPP forms. For this, the cDNA of human ppIAPP, pIAPP, matIAPP, SP with a GFP-tag were cloned into the multicopy vector p426-GAL1 under the control of the yeast *GAL1*-inducible promoter. A construct encoding the GFP tag was also generated for control purposes. The use of GFP tag allows easy detection of recombinant proteins, increases protein stability, and exacerbates protein aggregation (Niedenthal et al, 1996). The use of the galactose inducible *GAL1* promoter allows a tight regulation of gene expression according to the carbon source available. Thus, in the presence of glucose, the *GAL1* promoter is repressed due to catabolic repression. Raffinose reduces the effect of catabolic repression but gene expression is only triggered in the presence of galactose. The plasmid backbone has the auxotrophic marker *URA3*, allowing the selection of transformed cells (**Figure III.1**).

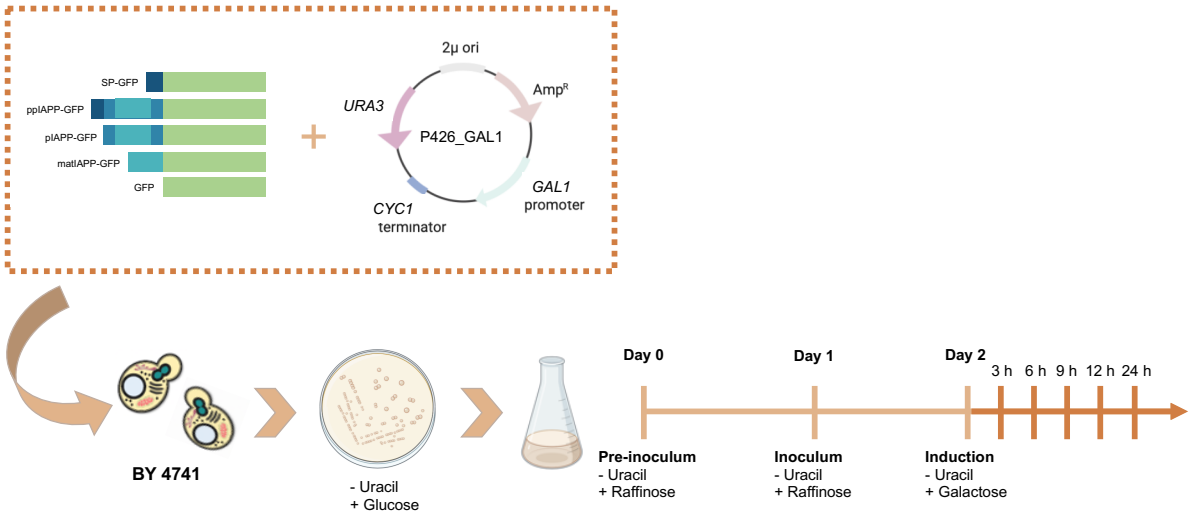

Figure III.1 – Schematic representation of human IAPP yeast models generation. The cDNA of human ppIAPP, pIAPP, matIAPP and SP, with and without a GFP tag were cloned into p426-GAL1. BY 4741 cells were transformed with the constructs and selected in solid media without uracil. SP-GFP = signal peptide-GFP, ppIAPP-GFP = preproIAPP-GFP, pIAPP = proIAPP-GFP, matIAPP = mature IAPP-GFP.

III.1.2 IAPP Forms Induce Toxicity in Yeast Cells

To verify if the constructs were being expressed, yeast strains were cultured and IAPP-GFP expression was induced with galactose. Analysis of the GFP signal was performed by flow cytometry in the indicated timepoints confirming that expression of all IAPP-GFP fusions generate a GFP^+ signal (**Figure III.2A**).

To evaluate viability, cells were stained with propidium iodide (PI) and analysed by flow cytometry (**Figure III.2B**). PI binds to double stranded DNA but it cannot permeate cells if plasma membrane is intact, allowing the determination of membrane integrity and consequently inferring cell viability. None of the constructs used as controls, p426 (empty vector), p426-GFP (GFP) and p426-SP-GFP (SP-GFP) affected cell viability up to 12 h of protein expression. Interestingly, cells expressing ppIAPP-GFP showed higher levels of toxicity after 12 and 24 h of induction with galactose, however SP-GFP was shown to be toxic at 24 h.

Considering that at 12 h there was similar GFP^+ for all strains, there is no toxicity of the controls and that 20.1 ± 5.0% of the yeast cells expressing ppIAPP-GFP were PI^+, compared to only 5.5 ± 0.8% or 5.6 ± 2.6% of cells expressing pIAPP-GFP or matIAPP-GFP, respectively, this timepoint was selected for further analysis.

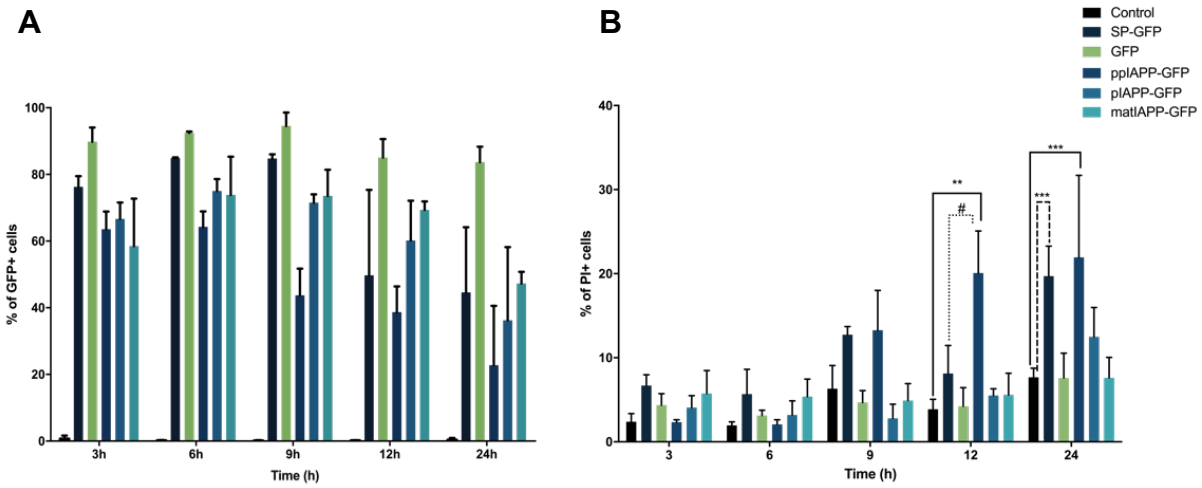

Figure III.2 – **Expression of preproIAPP mediated toxicity in yeast**. BY4741 cells expressing IAPP-GFP fusions and the respective controls were induced with galactose for the indicated time points and the frequency of (**A**) GFP positive cells and (**B**) propidium iodide (PI) positive cells was assessed by flow cytometry. Values represent mean ± standard deviation (SD) from at least three independent experiments. Statistical differences are represented as **p<0.01 and ***p<0.001 *vs* the control condition; #p<0.05 vs SP-GFP**.** SP-GFP = signal peptide-GFP, ppIAPP-GFP = preproIAPP-GFP, pIAPP-GFP = proIAPP-GFP, matIAPP-GFP = mature IAPP-GFP.

III.1.3 Effects of IAPP Expression on Yeast Cellular Growth

To investigate the effects of the constructs on cellular growth, spot assays were performed. The strains were consecutively diluted and plated onto repressing (glucose) or inducing (galactose) medium and incubated for 48 h (**Figure III.3**). Remarkably, all strains expressing IAPP in fusion with GFP showed compromised cellular growth when compared to the control, being this effect more pronounced in cells expressing ppIAPP-GFP.

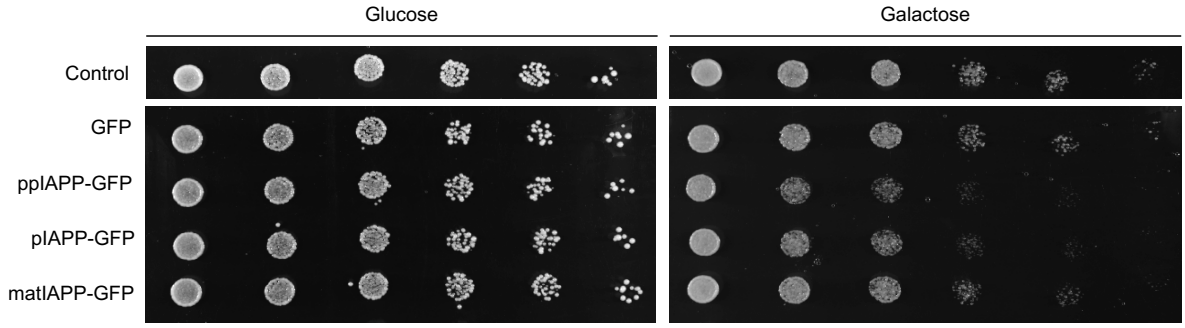

Figure III.3 – Expression of ppIAPP in yeast impairs cellular fitness. Cell suspensions were adjusted to the same OD_{600} and serially diluted and spotted onto the surface of solid medium containing either glucose or galactose and incubated for 48 h. A representative image is shown. ppIAPP-GFP = preproIAPP-GFP, pIAPP-GFP = proIAPP-GFP, matIAPP-GFP = mature IAPP-GFP.

Additionally, growth curve analysis were performed for each strain (**Figure III.4**). A normalized number of cells were induced by galactose and cell growth was monitored hourly for 24 h. Yeast cell growth is divided in three phases – lag phage, exponential phase and stationary phase. Cell cultures showed a short lag phase, corresponding to growth adaptation on galactose as the only carbon source. The duration of this phase depends on different environmental conditions like temperature, pH, oxygen, nutrients, etc. Once the cells start to divide, the exponential phase begins and growth was similar among strains for the first 5 h, when growth of the ppIAPP-GFP strain was slightly compromised when compared to the control. After 9 h the differences were more evident. For cells expressing pIAPP-GFP this effect could only be slightly detected at 12 h and for matIAPP-GFP there was no visible growth defects.

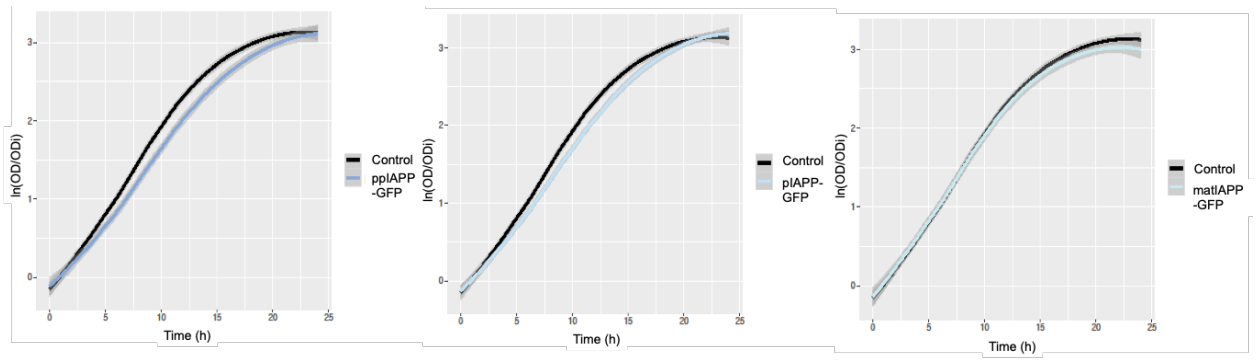

Figure III.4 – Expression of ppIAPP in yeast impairs cellular growth. Cell suspensions were adjusted to OD_{600} = 0.1 and incubated for 25 h at 30 ºC. A representative image is shown. ppIAPP-GFP = preproIAPP-GFP, pIAPP-GFP = proIAPP-GFP, matIAPP-GFP = mature IAPP-GFP.

III.2 IAPP Processing and Aggregation in Yeast

III.2.1 IAPP Intracellular Expression

To investigate IAPP expression and processing, immunoblotting assays were performed using antibodies against IAPP and GFP. To this end, cell lysates were prepared using TBS buffer after 12 h induction with galactose.

As indicated in **Figure III.5A**, protein levels were different among constructions. A signal of ~ 37 kDa was detected in cells expressing ppIAPP-GFP, which matches the full-length construct's molecular weight. Moreover, in cells expressing ppIAPP-GFP, two additional signals were detected, one of ~ 32 kDa and another of ~ 75 kDa. Likewise, pIAPP-GFP expressing-cells showed a ~ 35 kDa signal, corresponding to the molecular weight of the pIAPP-GFP construct. Additional signals of ~ 32 kDa and ~ 70 kDa were also detected in this condition. Lastly, for total protein lysates of mature IAPP-GFP, there was only a single signal of ~ 31 kDa, matching this construction's molecular weight. Furthermore, the membranes incubated with anti-GFP antibody showed a ~ 60 kDa signal in cells expressing matIAPP-GFP.

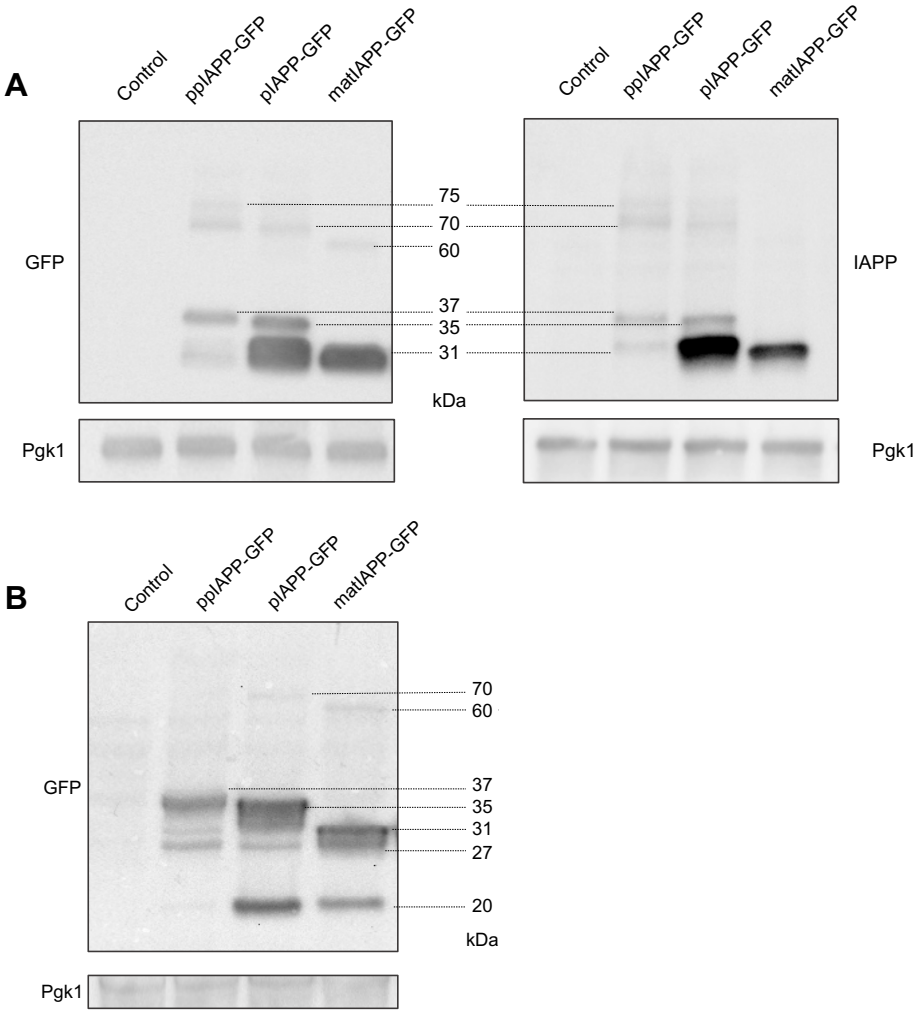

Figure III.5 – **IAPP is partially processed in yeast**. Cells expressing IAPP-GFP fusions and the control construct were induced with galactose for 12 h and protein lysates were obtained using (**A**) TBS buffer or (**B**) TCA buffer. Expression was assessed by immunoblotting using anti-IAPP and anti-GFP antibodies. Pgk1 was used as loading control. Representative images are shown. ppIAPP-GFP = preproIAPP-GFP, pIAPP-GFP = proIAPP-GFP, matIAPP-GFP = mature IAPP-GFP.

Additionally, cell lysates were also prepared using TCA after 12 h of induction with galactose. As observed in **Figure III.5B**, the results were similar to those observed for the protein lysates obtained with TBS. However, there was also a lower weight signal of ~ 20 kDa that may correspond to a processed form of GFP.

III.2.2 IAPP Aggregation

To investigate the sub-cellular distribution of IAPP, cells were observed by confocal fluorescence microscopy after induction with galactose for 12 h. As depicted in **Figure III.6**, the expression of all IAPP fusions induced the formation of IAPP aggregates with different morphology, at least in ppIAPP-GFP expressing cells. In this case, most of the fluorescent cells showed a heterogeneous distribution of intracellular aggregates. For cells expressing pIAPP-GFP and matIAPP-GFP, the fluorescence was scattered throughout the cell and there were mostly bigger and less defined aggregates. What appears to be the vacuole compartment was visible in these cells, with some cells presenting what looks to be intravacuolar aggregates.

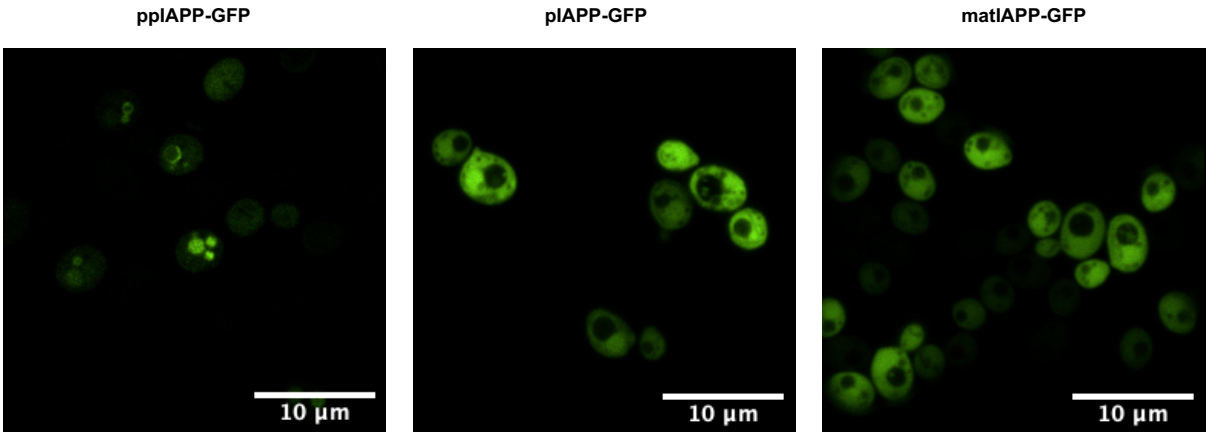

Figure III.6 – Expression of IAPP-GFP fusions induces the formation of aggregates with different morphologies. Cells were induced with galactose for 12 h and processed for fluorescence microscopy. Scale bar correspond to 10 µm. Representative images are shown. ppIAPP-GFP = preproIAPP-GFP, pIAPP-GFP = proIAPP-GFP, matIAPP-GFP = mature IAPP-GFP.

To further support that the structures observed in the fluorescence microscopy were IAPP aggregates, filter trap assays were performed. By filtering the cell lysates through a nitrocellulose membrane with 0.2 µm pores, this analysis allows the detection of intracellular aggregates higher than the cut-off of the membrane. As shown in **Figure III.7**, cells expressing pIAPP-GFP presented a stronger signal when compared to the other conditions, revealing the presence of high amounts of IAPP SDS-insoluble aggregates bigger than 0.2 µm in these cell lysates.

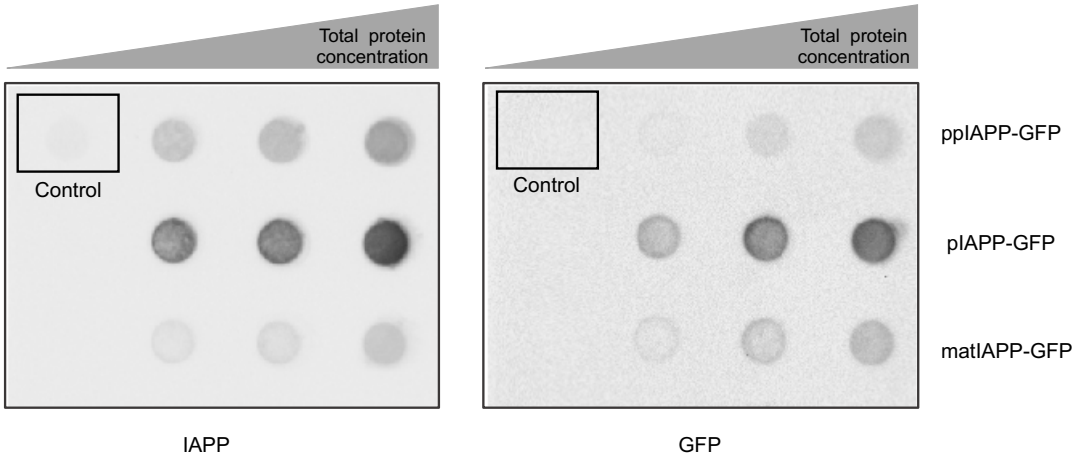

Figure III.7 – Immature IAPP-GFP fusions form aggregates with different sizes. Cells were induced for 12 h with galactose, subjected to filter trap assays and incubated with anti-IAPP and anti-GFP antibodies. Representative image is shown. ppIAPP-GFP = preproIAPP-GFP, pIAPP-GFP = proIAPP-GFP, matIAPP-GFP = mature IAPP-GFP.

III.2.3 IAPP Secretion

To evaluate the presence of IAPP fusions in the extracellular medium, cells were induced with galactose for 6 h and the media was collected. This timepoint was chosen as no significant cell death were detected (**Figure III.2B**), which could lead to the misinterpretation of the results derived from the release of IAPP as a consequence of cell death. Protein extracts were subjected to immunoblotting analysis using antibodies against IAPP and GFP (**Figure III.8**). A signal of ~ 37 kDa is detected in cells expressing ppIAPP-GFP, which matches the molecular weight the full-length construct. Likewise, pIAPP-GFP expressing-cells showed a ~ 35 kDa signal, corresponding to the molecular weight of pIAPP-GFP construct. For total protein lysates of mature IAPP-GFP, there is only a single signal of ~ 31 kDa, matching the molecular weight of this construction. Furthermore, the membranes incubated with anti-IAPP antibody showed a ~ 15 kDa signal in pIAPP-GFP constructs that can correspond to intermediate processing forms where GFP was cleaved. The membranes incubated with anti-GFP antibody showed a ~ 26 kDa and ~ 21 kDa signals in ppIAPP-GFP condition. This low molecular weight signals possibly correspond to the GFP form alone and to an intermediate processing form.

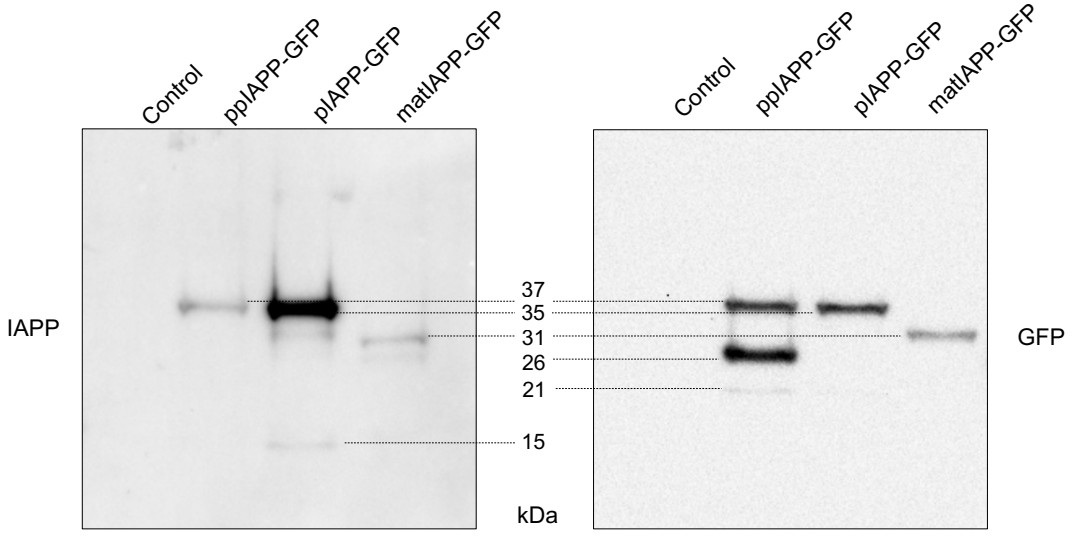

Figure III.8 – Release of IAPP-GFP fusions to the extracellular media. Cells were induced with galactose for 6 h, the media was collected and protein expression was assessed by immunoblotting using anti-IAPP and anti-GFP antibodies. Representative image is shown. ppIAPP-GFP = preproIAPP-GFP, pIAPP-GFP = proIAPP-GFP, matIAPP-GFP = mature IAPP-GFP.

III.3 Evaluation of Potential Protective Actions of TUDCA and UDCA Chaperones

III.3.1 Effect of TUDCA on Yeast Viability

The potential protective action of the chemical chaperone TUDCA in the viability of cells expressing IAPP-GFP fusions was evaluated by flow cytometry analysis using PI. As shown in **Figure III.9A**, the pattern of GFP expression was similar to that observed in **Figure III.2A**. ppIAPP-GFP expressing cells presented the lowest percentage of GFP^+ cells in all the concentrations tested, while cells expressing pIAPP-GFP and matIAPP-GFP showed similar levels. The increased percentage of PI^+ ppIAPP-GFP cells was not significantly affected by treating the cells with TUDCA in a concentration range of 100-500 μM (**Figure III.9B**).

III.3.2 Effect of UDCA on Yeast Viability

As TUDCA did not mediate cellular protection in ppIAPP-GFP expressing cells, it was hypothesized that the lack of a protective effect could be related to the low permeability of the compound to yeast cell wall. Thus, the potential protective action of UDCA, lacking the taurine moiety, was tested by flow cytometry analysis. As shown in **Figure III.10**, preliminary data indicated that UDCA treatment did not reduce cytotoxicity of ppIAPP-GFP in a concentration range of 10-250 μM.

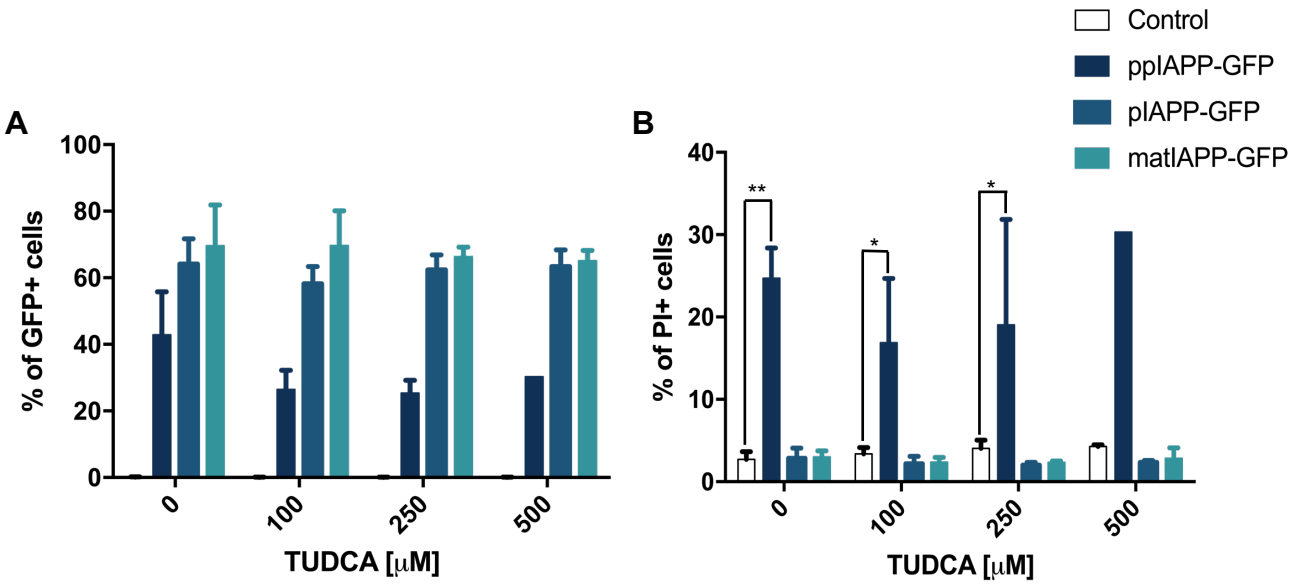

Figure III.9 – TUDCA does not protect yeast against IAPP-induced toxicity. Cells expressing IAPP-GFP fusions and the respective control were induced with galactose for 12 h and the frequency of (**A**) GFP positive cells and (**B**) propidium iodide (PI) positive cells was assessed by flow cytometry. Values represent mean ± standard deviation (SD) from at least three independent experiments. Statistical differences are represented as *p<0.05 and **p<0.01 *vs* the control condition. TUDCA = taurineursodeoxycholic acid, ppIAPP-GFP = preproIAPP-GFP, pIAPP-GFP = proIAPP-GFP, matIAPP-GFP = mature IAPP-GFP.

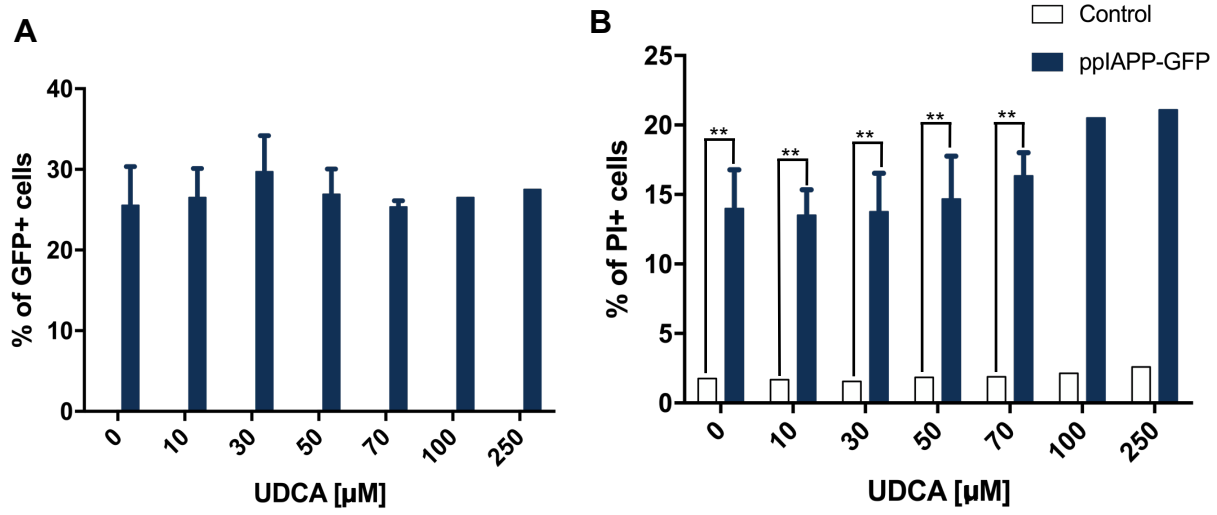

Figure III.10 – UDCA does not protect yeast against IAPP-induced toxicity. Cells expressing ppIAPP-GFP and the control were induced with galactose for 12 h and the frequency of (**A**) GFP positive cells and (**B**) propidium iodide (PI) positive cells was assessed by flow cytometry. Values represent mean ± standard deviation (SD) from at least three independent experiments. Statistical differences are represented as **p<0.01 *vs* the control condition. UDCA = ursodeoxycholic acid, ppIAPP-GFP = preproIAPP-GFP.

III.4 Generation of INS-1 832/13 β-Cell Line Stably Expressing hIAPP

The first steps on the generation of INS-1 832/13 β-cell line encoding the full-length hIAPP cDNA was previously performed in the laboratory. First, the cells were transfected with pCMV-blast-TET3G vector, obtained by replacing the neomycin resistance gene of pCMV-TET3G by the blasticidin resistance gene. Five clones were obtained, expanded and tested for GSIS. Clone 5 showed the closest results to the expected physiological response, i.e. there was an increased insulin secretion in response to hyperglycaemia (15 mM glucose) in comparison to the basal insulin secretion levels (3 mM glucose). Diazoxide blocks insulin secretion, serving as control for a true basal insulin secretion level that should be equivalent to insulin secretion levels at 3 mM glucose. Thus, clone 5 was selected for further modifications (**Table III.1**).

Table III.1 - Glucose-stimulated insulin secretion (GSIS) of INS-1 832/13 clones.

Glucose Treatment	***3 mM***	***15 mM***	***3 mM + Diazoxide [200 μM]***
Clones	Insulin (ng/mL)		
1	35.09	149.84	87.17
2	114.38	53.69	704.94
4	41.78	38.30	62.59
5	44.19	70.42	33.71
7	77.86	49.11	18.31

The cDNAs of ppIAPP-GFP and GFP were cloned into the vector pTRE3G-IRES vector using the In-Fusion HD cloning system. Clone 5-cells were transfected with ppIAPP-GFP or GFP and the hygromycin linear marker to select the positive clones (**Figure III.11**). Given the low transfection efficiency of pancreatic β-cells, only few hygromycin resistant colonies were obtained for each construct. However, no GFP signals were detected by fluorescence microscopy and immunoblotting after induction of cells with the tetracycline analogue doxycycline.

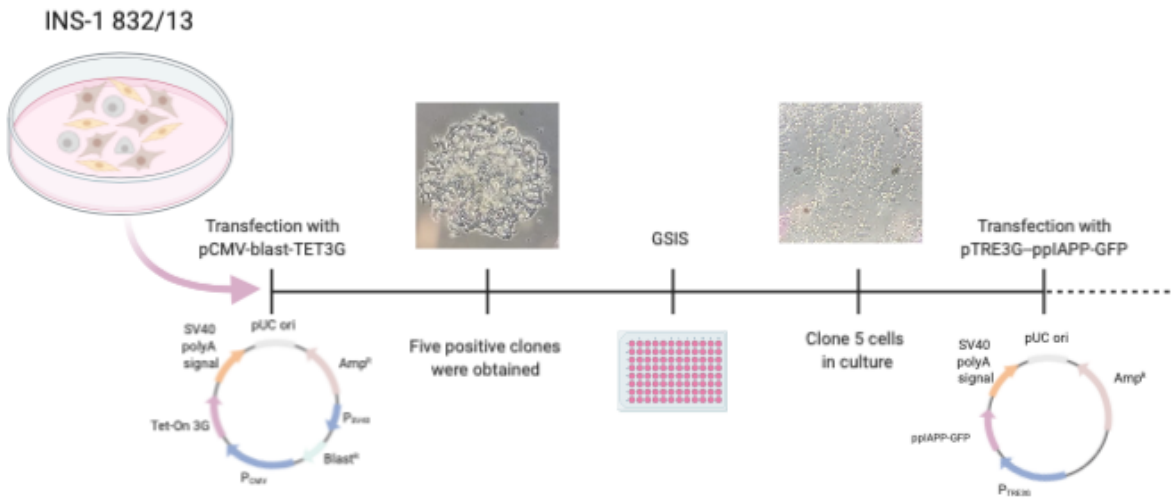

Figure III.11 – Schematic representation of the procedures for the generation of INS-1 832/13 β-cell line stably expressing ppIAPP-GFP. INS-1 832/13 cells were cultured and transfected with pCMV-blast-TET3G. Five clones were isolated, were subjected to GSIS and Clone 5 was selected. Clone 5-cells were transfected with the cDNA for ppIAPP-GFP or GFP alone together with a linear hygromycin marker for selection. ppIAPP-GFP = preproIAPP-GFP, blast = blasticidin, GSIS = glucose-stimulated insulin secretion. Image created with BioRender.com.

III.5 HeLa Tet-On Cell Line – an Alternative Approach

The HeLa Tet-On cell line was used as an alternative approach to investigate the pathological effects of immature hIAPP. HeLa Tet-On 3G cell line is derived from a human cervical epithelioid carcinoma that expresses the tetracycline (Tet)-regulated transactivator Tet-On 3G. This cell line, stably expressing the transactivator protein, was transiently transfected with the ppIAPP-GFP construct, and the respective vector and GFP controls. Protein expression was induced for 24 h with doxycycline and cells were observed under fluorescence microscopy (**Figure III.12**). Only cells transfected with the GFP alone displayed fluorescence signals, indicating that the GFP construct was working properly, while cells transfected with ppIAPP-GFP showed no detectable fluorescence signals.

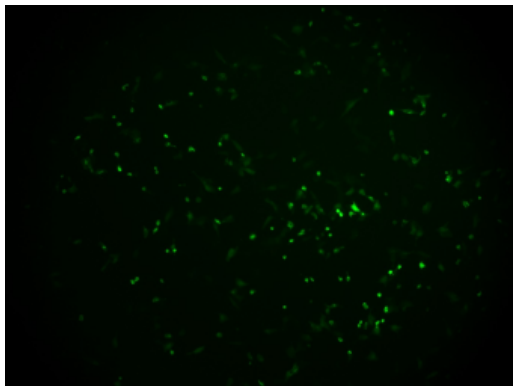

Figure III.12 – HeLa Tet-On cells expressing GFP. HeLa Tet-On cells were transfected with pTRE3G-GFP, GFP expression was induced with doxycycline for 24 h and fluorescence was monitored by fluorescence microscopy.

To verify if the constructs were properly expressed, cells were induced with doxycycline for 24 h, proteins were extracted with RIPA buffer and the media was also collected to monitor the secretion of hIAPP to the extracellular medium. Immunoblotting assays were performed using anti-IAPP and anti-GFP antibodies. As depicted in **Figure III.13**, a signal of ~ 37 kDa was detected in cells expressing ppIAPP-GFP, both with anti-IAPP and anti-GFP antibodies which matched the molecular weight of the full-length construct. This signal was also found in the cell media. A signal of ~ 27 kDa, corresponding to GFP alone, was also detected in cell lysates and in the media.

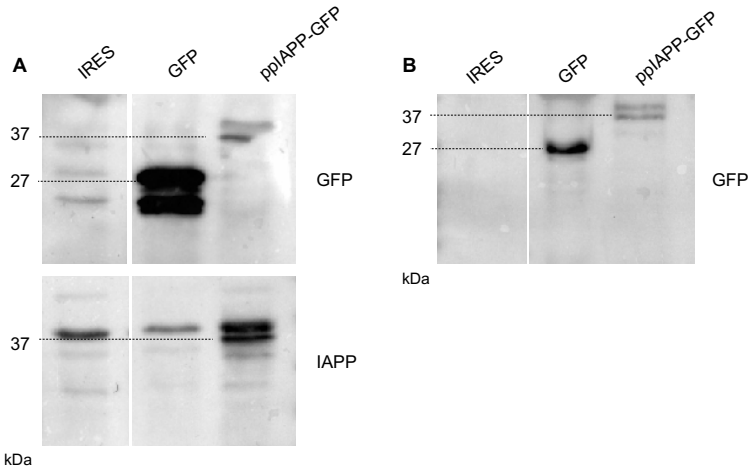

Figure III.13 – HeLa Tet-On cells properly express GFP and ppIAPP-GFP. HeLa Tet-On encoding ppIAPP-GFP and the respective controls were induced with doxycycline for 24 h and GFP and ppIAPP-GFP levels in cell lysates (**A**) and in the medium (**B**) were assessed by immunoblotting using anti-IAPP and anti-GFP antibodies. ppIAPP-GFP = preproIAPP-GFP. Representative images are shown.

To verify if ppIAPP-GFP expression affected cell metabolic capacity, Cell Titer-Blue® Cell viability assays were performed after ppIAPP-GFP expression was induced for 24 h with doxycycline. This method allows monitoring of cell viability based on the ability of living cells to convert a redox dye into a fluorescent end product. Although not statistically significant, the results showed a tendency in the decrease of viability of cells expressing ppIAPP-GFP (**Figure III.14**).

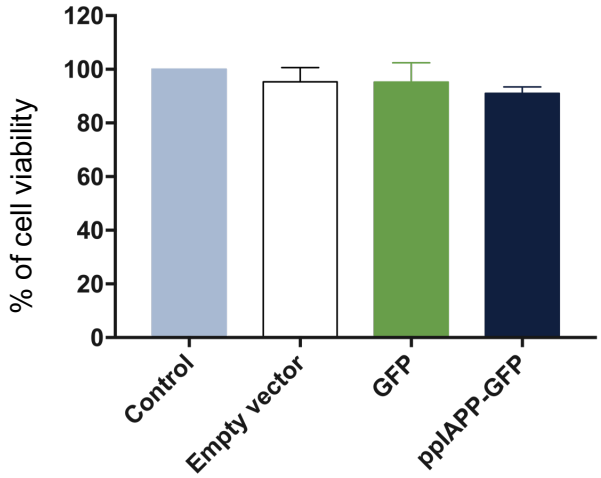

Figure III.14 – **Effect of ppIAPP-GFP expression in HeLa Tet-On cell viability**. Cells were transfected with the empty vector, GFP and ppIAPP-GFP and induced for 24 h with doxycycline. The Cell Titer-Blue® reagent was added to the media and cells were incubated for 1 h. Readings were done at 560/590 nm and values were normalized to the control cells. No statistically significant differences are observed between the conditions. ppIAPP-GFP = preproIAPP-GFP.

IV. DISCUSSION

Diabetes affects millions of people worldwide highlighting the need to develop new strategies to minimize the deleterious effects of this disease. Since IAPP was first discovered and linked to β-cell loss, it has been the subject of several studies. The relevance of hIAPP proteotoxicity for diabetes pathophysiology makes it an attractive target for the design of new strategic therapies aiming at the amelioration of disease pathological processes. Nevertheless, the underlying mechanisms of IAPP aggregation and toxicity in pancreatic β-cells are not yet fully understood, leaving room for further investigations.

This study first investigated the pathological role of immature human IAPP in yeast models expressing different IAPP forms, with focus on the role of immature IAPP on aggregation and cytotoxicity (Task 1). The lack of models allowing the study of hIAPP processing defects and the pathological consequences of the accumulation of immature intermediates on the formation of intracellular aggregates constitutes a limitation in the field. Over time, several studies have showed the unprecedented potential of yeasts as the simplest eukaryotic models to investigate the disease mechanisms (Menezes et al., 2015; Smith & Snyder, 2006). Remarkably, yeast has been very useful to study different aspects of protein misfolding diseases (Tenreiro & Outeiro, 2010).

The yeast models used in this study were generated by the heterologous expression of hIAPP constructs in multicopy yeast vectors to drive high levels of gene expression (**Figure III.1**). The inherent instability in the transmission of this extra-chromosomic DNA elements through generations can affect plasmid copy number, which can have minor effects on the results. A set of constructs drives the expression of IAPP-GFP fusion proteins. GFP has been widely used as a reporter protein to investigate protein expression and subcellular dynamics. Nevertheless, GFP also has some disadvantages as it can also aggregate in some circumstances and lead to cellular toxicity (Jensen, 2012; Niedenthal et al., 1996). On the other hand, strains expressing GFP-tagged hIAPP versions, particularly those expressing the immature forms, mediated significant cytotoxicity. This fact suggests that GFP enhances hIAPP cytotoxicity. However, GFP alone did not significantly affect cellular viability so the constructs with a GFP tag were chosen for further analysis.

The expression of hIAPP fusion proteins was first followed by assessing GFP^+ cells through flow cytometry (**Figure III.2A**). The deviations observed were probably due to variations in plasmid copy number. In general, the percentage of fluorescent cells seems to decrease with time for most of the constructs. This could be explained by different reasons. First, the increase of cell death observed over time, where GFP is degraded and/or released to the extracellular media in response to membrane leakage. Second, it may also result from GFP cleavage by yeast endoproteases acting on the IAPP sequence. Third, the accumulation of GFP in differently shaped aggregated species, as later confirmed by microscopy, may interfere with the signal acquisition in flow cytometry analysis. Moreover, the percentage of GFP^+ cells is lower for IAPP constructs than for the GFP controls, particularly for ppIAPP-GFP, suggesting that this protein is indeed present at lower levels as confirmed by immunoblotting analysis. Cell death increases over time for cells expressing IAPP, particularly for ppIAPP-GFP from 12 h incubation in the presence of galactose (**Figure III.2B**). These results suggest that the constructs were properly expressed, although they presented a variable expression patterns among strains and

over time. Starting from 12 h, ppIAPP-GFP expressing cells show a decrease in cell viability, suggesting a greater cytotoxic effect of this IAPP form. Importantly, until 12 h of induction, none of the controls were significantly toxic. However, at 24 h SP-GFP showed a relevant increase in cellular toxicity. This can be due the fact that the signal peptide of SP-GFP drives its translocation and accumulation in the ER, clogging the ER pathway and affecting vital cellular functions.

To investigate the impact of IAPP overexpression in yeast growth, phenotypic assays were performed (**Figure III.3**). A dramatic reduction in the growth of cells expressing ppIAPP-GFP, as compared to the control, may reflect the impairment of cellular functions, probably due to the toxic effect of immature forms of IAPP. Although expression of pIAPP-GFP and matIAPP-GFP did not seem to compromise significantly cell viability, as indicated before by the flow cytometry analysis, these constructs do interfere with cellular growth. Growth curve analysis corroborated that cells expressing immature IAPP forms showed impaired cellular growth (**Figure III.4**). Remarkably, and in accordance with the reduction of cell viability observed in flow cytometry, after 9 h induction with galactose the growth defects of cells expressing IAPP forms are evident. Interestingly, cells expressing ppIAPP-GFP showed a higher degree of growth impairment.

Altogether, these results show that expression of the three IAPP forms (ppIAPP-GFP, pIAPP-GFP, and matIAPP-GFP) are toxic to yeast cells at different degrees. Importantly, the immature ppIAPP-GFP form, appears to be the most toxic. Accumulation of these species may cause the overload of cell processing machinery and promote protein aggregation, interfering with key cellular pathways and ultimately leading to cell death.

To unveil the mechanisms behind the IAPP-induced toxicity in yeast, immunoblotting assays were performed. Protein lysates were generated using two buffers, TBS and TCA. Extraction with TBS buffer is less aggressive, preserving protein biochemical features, while TCA is more aggressive, causing protein precipitation and complete loss of structure. In both cases, total proteins in the cell lysates were separated on denaturing SDS-PAGE and similar results were obtained. Protein levels of ppIAPP-GFP, pIAPP-GFP, and matIAPP-GFP were shown to vary among strains, although there were no significant differences in the number of GFP^+ cells obtained by the flow cytometry analysis.

In protein lysates prepared with TBS (**Figure III.5A**), for each strain there is a signal that corresponds to the expected molecular weight of the construct. Curiously, the ~ 31 kDa signal, present in all IAPP-expressing cell, but more pronounced in pIAPP-GFP, suggesting that yeast endoproteases may process immature forms. Additionally, a signal of ~ 75 kDa was detected in cells expressing ppIAPP-GFP. Equivalent signals were detected for pIAPP-GFP and matIAPP-GFP, of ~ 70 and ~ 60 kDa, respectively. These high molecular weight signals may correspond to dimers or oligomeric species that were not completely denatured.

For the TCA-based protein extraction and incubation with anti-GFP antibody, the results are consistent with those described above (**Figure III.5B**). The high molecular weight bands are very faint, possibly due to the destabilization of molecular interactions between dimers or oligomers. Moreover, an additional signal of ~ 20 kDa was detected in protein lysates from pIAPP-GFP and matIAPP-GFP that may correspond to a fragment of GFP fused to the C-terminal flanking peptide. Additionally, a ~ 27 kDa signal was present in all IAPP-expressing strains that probably corresponds to GFP alone.

Altogether, these results suggest that IAPP forms can suffer alterations and processing in yeast cells. Considering that yeast encodes for endogenous convertases such as Kex2 (Fuller et al., 1989; Kjeldsen, 2000), ppIAPP and pIAPP peptides may be recognized and cleaved by these enzymes. Immunoreactive signals of lower molecular weight may correspond to processing intermediates and giving rise to peptides like GFP fused to the C-terminal flanking peptide located downstream of the PC1/3 cleavage site both in ppIAPP and pIAPP (**Figure I.5B**).

The identity of the high molecular weight protein species detected in the immunoblotting assays was confirmed by nanoLC-MS/MS. Results showed that specific sequences of IAPP and GFP, namely, the internal IAPP and C-terminal of pIAPP fused to GFP sequences were detected in samples from ppIAPP-GFP and pIAPP-GFP (Raimundo et al., 2020). This further supports the hypothesis that endogenous yeast convertases process IAPP immature species.

Since the results obtained for immunoblotting suggested the presence of intracellular aggregates in IAPP-expressing yeast, the cells were observed under fluorescence microscopy to monitor the presence of aggregates (**Figure III.6**). In general, most fluorescent cells presented intracellular aggregates. Noteworthy, cells expressing pIAPP-GFP and matIAPP-GFP showed a more diffused fluorescence pattern with less defined aggregates. An apparent predominance of aggregates in the compartment presumed to be the vacuole appeared to occur in these cells. Accumulation of intravacuolar aggregates may be a possible explanation for the lack of toxicity. On the other hand, for ppIAPP-GFP expressing cells, the fluorescence is more heterogeneously distributed with well-defined aggregates. These differences seem to be associated with the impaired growth and viability for ppIAPP-GFP strain. The formation and accumulation of intracellular aggregates may explain the decrease in cell viability observed over time. Furthermore, the different subcellular localization of aggregates in the different strains may be related to the different toxicities observed. Although there is an indication of a possible co-localization of the aggregates in the vacuole, further analyses are necessary to confirm this hypothesis. Under stress conditions, the compartmentalization of toxic elements (in this case toxic protein aggregates) into vacuole is used by cells as a protective mechanism to avoid further damaging of cellular functions. In the case of ppIAPP-GFP, the signal is more scattered throughout the cell, which indicated that they are available in the cytosol to interfere with cellular functions justifying the increased toxicity observed in this strain.

The frequency of cells showing IAPP-GFP aggregates and the aggregate's area were also calculated (Raimundo et al., 2020). The frequency of GFP^+ cells corroborated the results obtained by flow cytometry analysis. ppIAPP-GFP cells displayed the higher number of cells with aggregates with the smaller average area when compared to the other two strains, which showed similar number of cells with aggregates. However, in terms of aggregate size distribution, pIAPP-GFP cells have mostly smaller aggregates, similar to ppIAPP-GFP, than matIAPP-GFP that presents a higher percentage of bigger aggregates (Raimundo et al., 2020). Altogether, these data support that small soluble aggregates are the drivers of IAPP-induced cytotoxicity.

To further validate these results, total protein lysates were subjected to filter-trap assays (**Figure III.7**) (Juenemann et al., 2015; Nasir et al., 2015; Cox & Ecroyd, 2017). Interestingly, lysates from pIAPP-GFP-expressing cells displayed the strongest signal, implying the presence of high

amounts of IAPP SDS-insoluble aggregates bigger than the membrane pore. On the other hand, lysates of cells expressing ppIAPP-GFP and matIAPP-GFP, showed a weaker signal. However, these results should be interpreted with caution, since the protein levels of the IAPP-GFP fusions are extremely variable among strains as mentioned before. Thus, the intense signal in pIAPP-GFP may just reflect a higher protein content. Nevertheless, these results are in agreement with the hypothesis that smaller aggregates are the drivers of cytotoxicity, instead of the bigger aggregates.

As mentioned before, ppIAPP-GFP appeared to have the lowest expression levels. One hypothesis to justify this is the possible secretion of ppIAPP-GFP to the extracellular media. ppIAPP-GFP bears the signal peptide responsible for the entry in the secretory pathway. To assess the presence of the constructs in the extracellular media, cells were induced for 6 h, when cellular death is still low as indicated by the flow cytometry data, meaning that the presence of IAPP in the media was not caused by membrane leakage (**Figure III.2B**). The presence of intracellular aggregates at this timepoint was confirmed by microscopy and it was similar to what was observed at 12 h (Raimundo et al., 2020). Immunoblotting analysis showed extracellular IAPP signals in all strains (**Figure III.8**). Additional low molecular weight signals might correspond to processing intermediates that were released to the extracellular media. Moreover, the presence of pIAPP-GFP and matIAPP-GFP in the extracellular media, suggests that the signals may result from basal cellular death or that pIAPP and matIAPP may enter the secretory pathway by alternative pathways. Also, the aggregation and accumulation of these species might cause them to be released from cells as a protective mechanism. Experiments using mutant strains with defects in the secretory pathway are needed to shed some light on this issue.

The accumulation of misfolded IAPP is also associated with ER stress, which can lead to cell death. IAPP synthesis starts in the ER. This organelle is crucial for protein synthesis and is very sensible to environmental changes and cellular stress, being very susceptible to factors affecting cell homeostasis and leading to ER stress (Chung et al., 2017). Several studies point ER stress as a critical mechanism involved in β-cell dysfunction and T2DM progression associated with extra- and intracellular IAPP aggregation (Huang et al., 2019). Therefore, it was hypothesized that chemical chaperones such as TUDCA and UDCA, that ameliorate ER stress, might have a protective role against the effects of IAPP aggregation.

TUDCA was the first compound to be tested as a previous study showed a reduction of ER stress markers in β-cells overexpressing hIAPP (Cadavez et al., 2014). Flow cytometry analysis showed no changes in GFP expression patterns, suggesting that TUDCA did not interfere with the protein level of GFP constructs or cause alterations in cell viability (**Figure III.9**). A possible explanation is that yeast have a cell wall that could prevent the compound to effectively enter the cells. To overcome this potential limitation, UDCA lacking the taurine moiety was tested as few studies show that it has a better permeability than TUDCA in animal cells (Martinez et al., 1998). Flow cytometry analysis showed no improvements in cell viability with UDCA treatment (**Figure III.10**). Altogether, the data from these experiments indicate that, although TUDCA and UDCA showed protective effects in animal cells, they have no apparent protective effect in IAPP-induced cytotoxicity in yeast, at least in the tested concentrations.

One of the goals of this study was the generation of an INS-1 832/13 β-cell line stably expressing immature hIAPP to investigate the molecular mechanisms underlying hIAPP proteotoxicity. INS-1 832/13 emerged as a useful tool since it brings advantages over the previously available cell lines. The glucose effect can be potentiated by different known agents and the glucose-induced insulin secretion is closer to physiologic levels. However, they also differ from normal islets in some fundamental aspects, namely in the glucose response threshold (lower than normal rat islets) and in maximum response to glucose (8 mmol/L unlike normal rat islets) (Hohmeier et al., 2000).

To this end, an inducible expression system was used (**Figure IV.1**). The INS-1 832/13 β-cells were transfected with a pCMV-TET3G vector that contains the gene for the transactivator protein, Tet-On 3G, under the regulation of a constitutive promoter. The positive clones stably express the Tet-On 3G transactivator protein that is highly sensitive to doxycycline (Zhou et al., 2006). Doxycycline is a synthetic tetracycline derivative and the most active analogue of tetracycline, therefore it is used as the effector molecule for the Tet-On Tet-Off systems. Five clones were obtained and glucose-stimulated insulin secretion (GSIS) was tested. GSIS allows the measurement of the cell's insulin secretion induced by glucose and only clone 5 showed closest results to the physiological response, so it was chosen to proceed for further analysis.

The cDNAs encoding for ppIAPP-GFP and GFP were cloned in the pTRE3G-IRES vector, in which the TRE3G inducible promoter (PTREG) regulates the transcription of target genes. This promoter has very low basal expression and maximal expression after induction and consists of 7 repeats of a 19 bp tet operator sequence located upstream of a minimal CMV promoter (Loew et al., 2010). When doxycycline is added to cell cultures, it binds to Tet-On 3G, which suffers a conformational change that allows it to bind to the tet operator sequences located in the PTRE3G. The transcription is activated, and the downstream gene of interest is expressed. In the absence of doxycycline, the transcription levels are virtually absent since TRE3G lacks binding sites for endogenous mammalian transcription factors.

Clone 5-cells were transfected with ppIAPP-GFP or GFP and the hygromycin linear marker to select the positive clones (**Figure III.11**). Given the low transfection efficiency of pancreatic β-cells, only a few hygromycin resistant colonies were obtained for each construct. Moreover, these cells did not

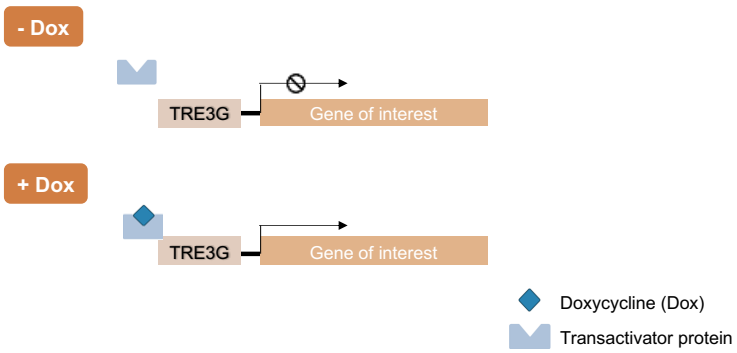

Figure IV.1 – Tet-ON 3G system allows inducible gene expression in the presence of doxycycline (Dox). Cells transfected with pCMV-TET3G vector constitutively express the transactivator protein. Then these cells were transfected with pTRE3G-IRES vector containing the gene of interest under a TRE3G dox-inducible promoter. In doxycycline absence, the transactivator protein is not activated and gene expression is not induced. When dox is present, it binds to the transactivator protein, promoting its binding to the promoter and activating the transcription of the gene of interest.

show any GFP signal detected by fluorescent microscopy or immunoblotting, after induction with doxycycline. However, the constructions were confirmed to be correct, so the low expression levels obtained may not be sufficient for detection by fluorescent microscopy or immunoblotting.

Thus, a possible alternative to overcome the low transfection efficiency of these cells might be to use lentivirus-mediated gene transfer. Lentiviruses have been widely used for gene delivery in many applications. It combines the use and speed of transient transfection with the robust expression in cell lines. These viruses can use the host machinery to amplify the transgene and delivery it to cells by membrane fusion (Elegheert et al., 2018).

As an alternative approach, the HeLa Tet-On cell line was used. This cell line originally expresses the transactivator protein Tet-On 3G. It was transiently transfected with the vectors encoding ppIAPP-GFP, GFP and the empty vector. After induction for 24 h with doxycycline, cells were observed under a fluorescence microscope and only GFP transfected cells exhibited a fluorescence signal (**Figure III.12**). To understand this result, ppIAPP-GFP and GFP levels were assessed immunoblotting (**Figure III.13**). A ~ 37 kDa signal matching the molecular weight of ppIAPP-GFP, both in cell lysates and in the media were detected, suggesting that proteins were properly expressed and partially secreted to the media. Thus, the absence of fluorescence may result from an alteration of GFP conformation that results in the loss of fluorescence signal, or that ppIAPP-GFP protein levels is under the detection threshold of the fluorescence microscope. Furthermore, cell metabolic capacity was also assessed using the Cell Titer-Blue® assay and suggests a tendency for the decrease in the viability for ppIAPP-GFP expressing cells, although the difference was not statistically significant (**Figure III.14**).

Overall, the data obtained indicate that the protocol for the overexpression of ppIAPP-GFP in INS-1 832/13 cells has many limitations and still needs optimization. Nevertheless, the development of a cell line model overexpressing immature forms of IAPP could be crucial to help unveil the mechanisms and pathways behind IAPP-induced cytotoxicity and β-cell dysfunction.

V. CONCLUSIONS AND PERSPECTIVES

Since IAPP was first discovered, its role in the pathophysiology of diabetes has been the subject of several studies, although the mechanisms underlying IAPP aggregation and toxicity are not yet completely understood. Initially, it was thought that IAPP extracellular deposition was responsible for pancreatic β-cell loss. However, it is currently accepted that intracellular small soluble oligomers and low-order aggregates of IAPP, which precedes amyloid deposition, are the main triggers of the cytotoxicity.

The data obtained in this study show that yeast expressing immature hIAPP forms display severe growth impairment. The accumulation of intracellular aggregates might interfere with crucial cellular pathways that cause the decrease of cellular viability.

Furthermore, the lack of hIAPP experimental models limits the investigation of the pathological mechanisms triggered by this peptide. Therefore, the development of models allowing the investigation of the impact of immature hIAPP forms on aggregation and proteotoxicity, will contribute to the development of new strategies capable of ameliorating the deleterious effects caused by IAPP aggregation.

Future studies, using mutants in the processing enzymes might shed more insights into the aggregation process and the pathological role of the different IAPP forms. Also, the use of yeast mutants with impairments in different proteostasis pathways for the expression of immature IAPP forms might allow the understanding of the triggers of cell death. At last, the identification of IAPP toxic species can lead to the development of new strategies and therapies that target and modulate IAPP aggregation.

VI. BIBLIOGRAPHY

Abedini A. & Schmidt A.M. (2013). Mechanisms of islet amyloidosis toxicity in type 2 diabetes. FEBS Letters, 587:1119-1127.

Ahlqvist E., Storm P., Käräjämäki A., Martinell M., Dorkhan M., Carlsson A., Vikman P., Prasad R., Aly D., Almgren P., Wessman Y., Shaat N., Spégel P., Mulder H., Lindholm E., Melander O., Hansson O., Malmqvist U., Lernmark A., Lahti K., Forsén T., Tuomi T., Resengren A. & Groop L. (2018). Novel subgroups of adult-onset diabetes and their association with outcomes: a data-driven cluster analysis of six variables. The lancet Diabetes & Endocrinology, 6:361-369.

Andersson L.E., Valtat B., Bagge A., Sharoyko V.V., Nicholls D.G., Ravassard P., Spégel P. & Mulder H. (2015). Characterization of stimulus-secretion coupling in the human pancreatic EndoC-βH1 beta cell line. PLoS One, 10:e0120879.

Anelli T. & Sitia R. (2008). Protein quality control in the early secretory pathway. The EMBO Journal, 27:315-327.

Ashcroft F.M. & Rorsman P. (2012). Diabetes mellitus and the β cell: the last ten years. Cell, 148:1160-1171.

Asthana S., Mallick B., Alexandrescu A.T. & Jha, S. (2018). IAPP in type ii diabetes: basic research on structure, molecular interactions, and disease mechanisms suggests potential intervention strategies. Biochimica et Biophysica Acta (BBA)-Biomembranes, 1860:1765-1782.

Barreto M., Kislaya I., Gaio V., Rodrigues A.P., Santos A.J., Namorado S., Antunes L., Gil A.P., Boavida J.M., Ribeiro R.T., Silva A.C., Prokopenko T., Nunes B., Dias C.M. & Vargas, P. (2017). Prevalence, awareness, treatment and control of diabetes in Portugal: results from the first national health examination survey (INSEF 2015). Diabetes Research and Clinical Practice, 140:271-278.

Baynes J.W. & Thorpe, S.R. (1999). Role of oxidative stress in diabetic complications: a new perspective on an old paradigm. Diabetes, 48:1-9.

Bennett R.G., Duckworth W.C. & Hamel F.G. (2000). Degradation of amylin by insulin-degrading enzyme. Journal of Biological Chemistry, 275:36621-36625.

Bratanova-Tochkova T.K., Cheng H., Daniel S., Gunawardana S., Liu Y.J., Mulvaney-Musa J., Schermerhorn T., Straub S.G., Yajima H. & Sharp G.W. (2002). Triggering and augmentation mechanisms, granule pools, and biphasic insulin secretion. Diabetes, 51:S83-S90.

Brereton M.F., Vergari E., Zhang Q. & Clark A. (2015). Alpha-, delta-and pp-cells: are they the architectural cornerstones of islet structure and co-ordination?. Journal of Histochemistry & Cytochemistry, 63:575-591.

Brissette M.J., Lepage S., Lamonde A.S., Sirois I., Groleau J., Laurin L.P. & Cailhier J.F. (2012). MFG-E8 released by apoptotic endothelial cells triggers anti-inflammatory macrophage reprogramming. PloS One, 7:e36368.

Bucciantini M., Giannoni E., Chiti F., Baroni F., Formigli L., Zurdo J., Taddei N., Ramponi G., Dobson C. M. & Stefani, M. (2002). Inherent toxicity of aggregates implies a common mechanism for protein misfolding diseases. Nature, 416:507-511.

Cadavez L., Montane J., Alcarraz-Vizán G., Visa M., Vidal-Fàbrega L., Servitja J.M. & Novials A. (2014). Chaperones ameliorate beta cell dysfunction associated with human islet amyloid polypeptide overexpression. PLoS One, 9:e101797.

Cao A.L., Wang L., Chen X., Wang Y.M., Guo H.J., Chu S., Liu C., Zhang X. & Peng, W. (2016). Ursodeoxycholic acid and 4-phenylbutyrate prevent endoplasmic reticulum stress-induced podocyte apoptosis in diabetic nephropathy. Laboratory Investigation, 96:610-622.

Chen Y.C., Taylor A.J. & Verchere C.B. (2018). Islet prohormone processing in health and disease. Diabetes, Obesity and Metabolism, 20:64-76.

Christmanson L., Rorsman F., Stenman G., Westermark P. & Betsholtz, C. (1990). The human islet amyloid polypeptide (IAPP) gene: organization, chromosomal localization and functional identification of a promoter region. FEBS Letters, 267:160-166.

Chung J., An S.H., Kang S. W. & Kwon K. (2016). Ursodeoxycholic acid (UDCA) exerts anti-atherogenic effects by inhibiting rage signalling in diabetic atherosclerosis. PLoS One, 11:e0147839.

Chung Y.R., Choi J.A., Koh J.Y. & Yoon Y.H. (2017). Ursodeoxycholic acid attenuates endoplasmic reticulum stress-related retinal pericyte loss in streptozotocin-induced diabetic mice. Journal of diabetes research, 2017.

Cobb, J. & Dukes, I. (1998). Recent advances in the development of agents for the treatment of type 2 diabetes. Annual reports in medicinal chemistry, 33:213-222.

Courtade J.A., Klimek-Abercrombie A.M., Chen Y.C., Patel N., Lu P.Y., Speake C., Orban P.C., Najafian B., Meneilly G., Greenbaum C.J., Panagiotopoulos C., Verchere C.B. & Warnock G.L. (2017). Measurement of pro-islet amyloid polypeptide (1–48) in diabetes and islet transplants. The Journal of Clinical Endocrinology & Metabolism, 102:2595-2603.

Cox D. & Ecroyd, H. (2017). The small heat shock proteins αB-crystallin (HSPB5) and Hsp27 (HSPB1) inhibit the intracellular aggregation of α-synuclein. Cell Stress and Chaperones, 22:589-600.

Deere D., Shen J., Vesey G., Bell P., Bissinger P. & Veal D. (1998). Flow cytometry and cell sorting for yeast viability assessment and cell selection. Yeast, 14:147-160.

Del Guerra S., Lupi R., Marselli L., Masini M., Bugliani M., Sbrana S., Torri S., Pollera M., Boggi U., Mosca F., Del Prato S. & Marchetti, P. (2005). Functional and molecular defects of pancreatic islets in human type 2 diabetes. Diabetes, 54:727-735.

Denroche H.C. & Verchere C.B. (2018). IAPP and type 1 diabetes: implications for immunity, metabolism and islet transplants. Journal of molecular endocrinology, 60:R57-R75.

Elegheert J., Behiels E., Bishop B., Scott S., Woolley R.E., Griffiths S.C., Byrne E., Chang V., Stuart D., Jones E., Aricescu A. & Siebold, C. (2018). Lentiviral transduction of mammalian cells for fast, scalable and high-level production of soluble and membrane proteins. Nature Protocols, 13:2991-3017.

Fernández M.S. (2014). Human IAPP amyloidogenic properties and pancreatic β-cell death. Cell Calcium, 56:416-427.

Froger A. & Hall J.E. (2007). Transformation of plasmid DNA into E. coli using the heat shock method. JoVE (Journal of Visualized Experiments), 6:e253.

Fu Z., Gilbert E.R. & Liu, D. (2013). Regulation of insulin synthesis and secretion and pancreatic beta-cell dysfunction in diabetes. Current diabetes reviews, 9:25-53.

Gasa R., Gomis R., Casamitjana R. & Novials A. (2001). High glucose concentration favors the selective secretion of islet amyloid polypeptide through a constitutive secretory pathway in human pancreatic islets. Pancreas, 22:307-310.

Gietz R.D. & Schiestl R.H. (1991). Applications of high efficiency lithium acetate transformation of intact yeast cells using single-stranded nucleic acids as carrier. Yeast, 7:253-263.

Green A.D., Vasu S. & Flatt P.R. (2018). Cellular models for beta-cell function and diabetes gene therapy. Acta physiologica, 222:e13012.

Guan H., Chow K., Shah R., Rhodes C. & Hersh L. (2012). Degradation of islet amyloid polypeptide by neprilysin. Diabetologia, 55:2989-2998.

Güemes M., Rahman S.A. & Hussain K. (2016). What is a normal blood glucose?. Archives of disease in childhood, 101:569-574.

Haase S.B. & Reed S.I. (2002). Improved flow cytometric analysis of the budding yeast cell cycle. Cell cycle, 1:117-121.

Haataja L., Gurlo T., Huang C.J. & Butler P.C. (2008). Islet amyloid in type 2 diabetes, and the toxic oligomer hypothesis. Endocrine reviews, 29:303-316.

Hofmann A.F. & Roda A. (1984). Physicochemical properties of bile acids and their relationship to biological properties: an overview of the problem. Journal of lipid research, 25:1477-1489.

Hohmeier H.E., Mulder H., Chen G., Henkel-Rieger R., Prentki M. & Newgard C.B. (2000). Isolation of INS-1-derived cell lines with robust ATP-sensitive K+ channel-dependent and -independent glucose-stimulated insulin secretion. Diabetes, 49:424-430.

Huang X.T., Liu W., Zhou Y., Sun M., Sun C.C., Zhang C.Y. & Tang S.Y. (2019). Endoplasmic reticulum stress contributes to NMDA-induced pancreatic β-cell dysfunction in a CHOP-dependent manner. Life Sciences, 232:116612.

Im E. & Martinez J.D. (2004). Ursodeoxycholic acid (UDCA) can inhibit deoxycholic acid (DCA)-induced apoptosis via modulation of EGFR/Raf-1/ERK signaling in human colon cancer cells. Journal of nutrition, 134:483-486.

International Diabetes Federation (2019). IDF Diabetes Atlas. 9th Ed. Brussels, Belgium: International Diabetes Federation.

Invernizzi P., Setchell K.D., Crosignani A., Battezzati P.M., Larghi A., O'Connell N.C. & Podda, M. (1999). Differences in the metabolism and disposition of ursodeoxycholic acid and of its taurine-conjugated species in patients with primary biliary cirrhosis. Hepatology, 29:320-327.

Jensen E.C. (2012). Use of fluorescent probes: their effect on cell biology and limitations. The Anatomical Record: Advances in Integrative Anatomy and Evolutionary Biology, 295:2031-2036.

Juenemann K., Wiemhoefer A. & Reits E.A. (2015). Detection of ubiquitinated huntingtin species in intracellular aggregates. Frontiers in molecular neuroscience, 8:1.

Kahm M., Hasenbrink G., Lichtenberg-Fraté H., Ludwig J. & Kschischo M. (2010). Grofit: fitting biological growth curves. Nature Precedings, 1-1.

Kahn S.E. (2003). The relative contributions of insulin resistance and beta-cell dysfunction to the pathophysiology of type 2 diabetes. Diabetologia, 46:3-19.

Kahn S.E., Hull R.L. & Utzschneider K.M. (2006). Mechanisms linking obesity to insulin resistance and type 2 diabetes. Nature, 444:840-846.

Kayatekin C., Amasino A., Gaglia G., Flannick J., Bonner J.M., Fanning S., Narayan P., Barrasa M., Pincua D., Landgraf D., Nelson J, Hesse W., Costanzo M., AMP T2D-GENES Consortium, Myers C., Boone J. & Lindquist S. (2018). Translocon declogger Ste24 protects against IAPP oligomer-induced proteotoxicity. Cell, 173:62-73.

Khurana V. & Lindquist S. (2010). Modelling neurodegeneration in Saccharomyces cerevisiae: why cook with baker's yeast?. Nature Reviews Neuroscience, 11:436-449.

Kleinert M., Clemmensen C., Hofmann S.M., Moore M.C., Renner S., Woods S.C., Huypens P., Beckers J., Angelis M., Schurmann A., Bakhti M., Klingenspor M., Heiman M., Cherrigton A., Ristow M., Lickert H., Wolf E., Havel P., Muller T. & Tschop M. (2018). Animal models of obesity and diabetes mellitus. Nature Reviews Endocrinology, 14:140.

Knight J.D., Williamson J.A. & Miranker A.D. (2008). Interaction of membrane-bound islet amyloid polypeptide with soluble and crystalline insulin. Protein Science, 17:1850-1856.

Knowles T.P., Vendruscolo M., & Dobson C.M. (2014). The amyloid state and its association with protein misfolding diseases. Nature reviews Molecular cell biology, 15:384-396.

Kucharska J., Braunova Z., Ulicna O., Zlatos L. & Gvozdjakova A. (2000). Deficit of coenzyme Q in heart and liver mitochondria of rats with streptozotocin-induced diabetes. Physiological research, 49:411-418.

Leckström A., Björklund K., Permert J., Larsson R. & Westermark, P. (1997). Renal elimination of islet amyloid polypeptide. Biochemical and biophysical research communications, 239:265-268.

Lee B., Udagawa T., Singh C.R. & Asano K. (2007). Yeast phenotypic assays on translational control. In Methods in enzymology, vol. 429 p.105-137. Academic Press.

Lin C.Y., Gurlo T., Kayed R., Butler A.E., Haataja L., Glabe C.G. & Butler P.C. (2007). Toxic human islet amyloid polypeptide (h-IAPP) oligomers are intracellular, and vaccination to induce anti-toxic oligomer antibodies does not prevent h-IAPP–induced β-cell apoptosis in h-IAPP transgenic mice. Diabetes, 56:1324-1332.

Loew R., Heinz N., Hampf M., Bujard H. & Gossen M. (2010). Improved Tet-responsive promoters with minimized background expression. BMC biotechnology, 10:81.

Lukivskaya O., Lis R., Egorov A., Naruta E., Tauschel H.D. & Buko V.U. (2004). The protective effect of ursodeoxycholic acid in alloxan-induced diabetes. Cell Biochemistry and Function: Cellular biochemistry and its modulation by active agents or disease, 22:97-103.

Lukivskaya O., Patsenker E. & Buko V.U. (2007). Protective effect of ursodeoxycholic acid on liver mitochondrial function in rats with alloxan-induced diabetes: link with oxidative stress. Lifes sciences, 80:2397-2402.

Macfarlane W.M., Campbell S.C., Elrick L.J., Oates V., Bermano G., Lindley K.J., Aynsley-Green A., Dunne M.J., James R.F.L. & Docherty, K. (2000). Glucose regulates islet amyloid polypeptide gene transcription in a PDX1-and calcium-dependent manner. Journal of Biological Chemistry, 275:15330-15335.

Madhavan A., Sindhu R., Arun K.B., Pandey A. & Binod P. (2018). Advances and tools in engineering yeast for pharmaceutical production. In Biosynthetic Technology and Environmental Challenges p. 29-49. Springer, Singapore.

Martinez J.D., Stratagoules E.D., LaRue J.M., Powell A.A., Gause P.R., Craven M.T., Payne C.M., Powell M.B., Gerner E.W. & Earnest D.L. (1998) Different bile acids exhibit distinct biological effects: the tumor promoter deoxycholic acid induces apoptosis and the chemopreventive agent ursodeoxycholic acid inhibits cell proliferation. Nutrition and Cancer, 31:111-118.

Marzban L., Trigo-Gonzalez G. & Verchere C.B. (2005). Processing of pro-islet amyloid polypeptide in the constitutive and regulated secretory pathways of β cells. Molecular endocrinology, 19:2154-2163.

Marzban, L., Rhodes, C. J., Steiner, D. F., Haataja, L., Halban, P. A., & Verchere, C. B. (2006). Impaired NH2-terminal processing of human proislet amyloid polypeptide by the prohormone convertase PC2 leads to amyloid formation and cell death. Diabetes, 55:2192-2201.

McGuckin E., Cade J.E. & Hanison J. (2020). The pancreas. Anaesthesia & Intensive Care Medicine.

Menezes R., Tenreiro S., Macedo D., Santos C.N. & Outeiro T.F. (2015). From the baker to the bedside: yeast models of Parkinson's disease. Microbial cell, 2:262.

Mukherjee A., Morales-Scheihing D., Butler P.C. & Soto C. (2015). Type 2 diabetes as a protein misfolding disease. Trends in molecular medicine, 21:439-449.

Mukherjee A., Morales-Scheihing D., Salvadores N., Moreno-Gonzalez I., Gonzalez C., Taylor-Presse K., Mendez N., Shahnawaz M., Gaber A.O., Sabek O.M., Fraga D.W. & Soto C. (2017). Induction of IAPP amyloid deposition and associated diabetic abnormalities by a prion-like mechanism. Journal of Experimental Medicine, 214:2591-2610.

National Diabetes Observatory. (2019, November 14). Dia Mundial da Diabetes – Dados preliminares do Observatório Nacional da Diabetes. Retrieved from https://www.spd.pt/#/comunicado-de-imprensa.

Ngoka L.C. (2008). Sample prep for proteomics of breast cancer: proteomics and gene ontology reveal dramatic differences in protein solubilization preferences of radioimmunoprecipitation assay and urea lysis buffers. Proteome science, 6:1-24.

Niedenthal R.K., Riles L., Johnston M. & Hegemann J.H. (1996). Green fluorescent protein as a marker for gene expression and subcellular localization in budding yeast. Yeast, 12:773-786.

Nishi M., Sanke T., Seino S., Eddy R.L., Fan Y.S., Byers M.G., Shows T.B., Bell G.I. & Steiner D.F. (1989). Human islet amyloid polypeptide gene: complete nucleotide sequence, chromosomal localization, and evolutionary history. Molecular Endocrinology, 3:1775-1781.

Outeiro T.F. & Lindquist S. (2003). Yeast cells provide insight into alpha-synuclein biology and pathobiology. Science, 302:1772-1775.

Outeiro T.F. & Muchowski P.J. (2004). Molecular genetics approaches in yeast to study amyloid diseases. Journal of Molecular Neuroscience, 23:49-59.

Özcan U., Yilmaz E., Özcan L., Furuhashi M., Vaillancourt E., Smith R.O., Gorgun C.Z. & Hotamisligil G. S. (2006). Chemical chaperones reduce ER stress and restore glucose homeostasis in a mouse model of type 2 diabetes. Science, 313:1137-1140.

Paulsson J.F., Andersson A., Westermark P. & Westermark G.T. (2006). Intracellular amyloid-like deposits contain unprocessed pro-islet amyloid polypeptide (proIAPP) in beta cells of transgenic mice overexpressing the gene for human IAPP and transplanted human islets. Diabetologia 49:1237-1246.

Press M., Jung T., König J., Grune T. & Höhn A. (2019). Protein aggregates and proteostasis in aging: amylin and β-cell function. Mechanisms of ageing and development, 177:46-54.

Raimundo A.F., Ferreira S., Farrim M.I., Santos C.N. & Menezes R. (2020). Heterologous Expression of Immature Forms of Human Islet Amyloid Polypeptide in Yeast Triggers Intracellular Aggregation and Cytotoxicity. Frontiers in Microbiology, 11:2035.

Raleigh D., Zhang X., Hastoy B. & Clark A. (2017). The β-cell assassin: IAPP cytotoxicity. Journal of molecular endocrinology, 59:R121-R140.

Rees D.A. & Alcolado J.C. (2005). Animal models of diabetes mellitus. Diabetic medicine, 22:359-370.

Rodrigues C.M., Fan G., Wong P.Y., Kren B.T. & Steer C.J. (1998). Ursodeoxycholic acid may inhibit deoxycholic acid-induced apoptosis by modulating mitochondrial transmembrane potential and reactive oxygen species production. Molecular medicine, 4:165-178.

Rorsman P. & Braun M. (2013). Regulation of insulin secretion in human pancreatic islets. Annual review of physiology, 75:155-179.

Schroeder L. & Ikui A.E. (2019). Tryptophan confers resistance to SDS-associated cell membrane stress in Saccharomyces cerevisiae. PloS one, 14:e0199484.

Sekhon S.S., Ahn J.Y., Shin W., Kim G., Yoon H., Min J. & Kim Y.H. (2015). Sample preparation for optimal proteomic profiling of rabbit muscle and tendon using radio-immunoprecipitation assay (RIPA) and urea lysis buffers. Toxicology and Environmental Health Sciences, 7:184-189.

Skelin M., Rupnik M. & Cencič A. (2010). Pancreatic beta cell lines and their applications in diabetes mellitus research. ALTEX-Alternatives to animal experimentation, 27:105-113.

Smith M.G. & Snyder M. (2006). Yeast as a model for human disease. Current protocols in human genetics, 48:15-6.

Stefani M. (2004). Protein misfolding and aggregation: new examples in medicine and biology of the dark side of the protein world. Biochimica et Biophysica Acta (BBA)-Molecular Basis of Disease, 1739:5-25.

Tenreiro S. & Outeiro T.F. (2010). Simple is good: yeast models of neurodegeneration. FEMS yeast research, 10:970-979.

Vettorazzi J.F., Ribeiro R.A., Borck P.C., Branco R.C.S., Soriano S., Merino B., Boschero A.C., Nadal A., Quesada I. & Carneiro E.M. (2016). The bile acid TUDCA increases glucose-induced insulin secretion via the cAMP/PKA pathway in pancreatic beta cells. Metabolism, 65:54-63.

Westermark P., Andersson A. & Westermark G.T. (2011). Islet amyloid polypeptide, islet amyloid, and diabetes mellitus. Physiological reviews, 91:795-826.

Wright A.P., Bruns M. & Hartley B.S. (1989). Extraction and rapid inactivation of proteins from Saccharomyces cerevisiae by trichloroacetic acid precipitation. Yeast, 5:51-53.

Xavier G.D.S. & Rutter G.A. (2020). Metabolic and functional heterogeneity in pancreatic β cells. Journal of molecular biology, 432:1395-1406.

Yoshida H. (2007). ER stress and diseases. The FEBS journal, 274:630-658.

Zhou X., Vink M., Klaver B., Berkhout B. & Das A.T. (2006). Optimization of the Tet-On system for regulated gene expression through viral evolution. Gene therapy, 13:1382-1390.

Zou X., Ouyang H., Yu T., Chen X., Pang D., Tang X. & Chen C. (2019). Preparation of a new type 2 diabetic miniature pig model via the CRISPR/Cas9 system. Cell death & disease, 10:1-10.

Zraika S., Hull R.L., Udayasankar J., Clark A., Utzschneider K.M., Tong J., Gerchman F. & Kahn S.E. (2007). Identification of the amyloid-degrading enzyme neprilysin in mouse islets and potential role in islet amyloidogenesis. Diabetes, 56:304-310.